

Efficient Variational Dynamics of Open Quantum Bosonic Systems via Automatic Differentiation

Jacopo Tosca,¹ Francesco Carnazza,¹ Luca Giacomelli,¹ and Cristiano Ciuti¹

¹*Université Paris Cité, CNRS, Matériaux et Phénomènes Quantiques, 75013 Paris, France*

(Dated: July 21, 2025)

We introduce a scalable variational method for simulating the dynamics of interacting open quantum bosonic systems deep in the quantum regime. The method is based on a multi-dimensional Wigner phase-space representation and employs a Variational Multi-Gaussian (VMG) ansatz, whose accuracy is systematically controlled by the number of Gaussian components. The variational equations of motion are derived from the Dirac–Frenkel principle and evaluated efficiently by combining the analytical structure of Gaussian functions with automatic differentiation. As a key application, we study a driven-dissipative two-dimensional Bose–Hubbard lattice with two-boson coherent driving and two-body losses. Using our dynamical approach, we compute the finite-size scaling of the Liouvillian spectral gap—extracted from the relaxation dynamics—which vanishes in the thermodynamic limit. Our results reveal critical slowing down with dynamical exponents of the 2D quantum Ising universality class, demonstrating the power of our method to capture complex quantum dynamics in large open systems.

Interacting open quantum bosonic systems lie at the heart of major efforts in both fundamental quantum science and emerging quantum technologies. This is particularly evident in the field of non-equilibrium quantum fluids of light, where photons acquire effective interactions and collective behavior in nonlinear media [1–3]. On the applied side, engineered platforms of interacting photons are being developed for quantum information processing, with a special focus on nonlinear systems that enable the deterministic generation of photonic Schrödinger-cat states [4–18].

Describing the dynamics of open quantum bosonic systems with a large number of modes remains highly nontrivial. The full quantum dynamics of interacting bosons—especially under non-equilibrium and dissipative conditions—poses severe challenges due to the infinite-dimensional Hilbert space of each mode, the presence of strong quantum correlations, and the need to capture both transient and steady-state behavior. Powerful methods, like those based on the Density Matrix Renormalization Group [19], Matrix Product States and Tensor Networks [20], have been applied to driven-dissipative settings mostly for spin lattices [21, 22], while open bosonic systems remains a more difficult hurdle. Other techniques, such as the corner-space renormalization method [23], use low-rank representations of the many-body density matrix and can reach accuracies comparable to exact diagonalization even with bosons. The Corner Space Renormalization approach has proven effective in describing non-equilibrium phase transitions [24]. Yet, it is constrained to steady-state properties and to systems with moderately low von Neumann entropy, which limits the size of the systems that can be simulated.

The emergence of machine learning approaches has sparked interest in Neural Quantum States [25]. These methods provide expressive variational *ansätze* for quantum many-body wavefunctions and have reached state-of-the-art performance in simulating ground states of lattice spin models and related systems [26–34]. However, ex-

tending them to bosonic statistics or continuous variables in driven-dissipative regimes has proven to be difficult. As emphasized on the recent work on bosons [34], “accurate neural representations of the density matrix are still unavailable” for such settings.

For bosonic systems, a natural representation of the many-body density matrix is provided by the Wigner function [35], which maps the quantum state to a quasiprobability distribution in phase space, with each bosonic mode described by a complex variable (or a pair of real quadratures). The time evolution of the Wigner function, governed by the Lindblad master equation, takes the form of a partial differential equation with higher-order derivatives with respect to the phase-space bosonic variables. Truncating these derivatives yields a Fokker–Planck-like equation that preserves positivity and can be sampled efficiently using classical trajectories. This so-called truncated Wigner approximation, however, breaks down in quantum regimes where the Wigner function becomes negative. This is the case for example when the system is in a so-called bosonic Schrödinger cat state [4, 5]. An alternative phase-space formalism is offered by the positive-P representation [36], which avoids truncation and allows for exact stochastic simulations. This method scales linearly with system size and is effective for weakly interacting bosons with strong dissipation. Yet, it fails to converge in regimes with strong quantum correlations or long-time evolution.

To date, no approach has succeeded in providing a scalable and accurate variational method in the fully quantum regime based on a phase-space representation. Nevertheless, a phase-space representation, being functional in nature, opens the door to using well-defined sets of analytical functions—potentially enabling exact manipulations even in regimes with strong negativities and correlations. In principle, this could be achieved with automatic differentiation techniques [37], a powerful and recent technique developed in computer science, which fully exploits modern computational parallel architec-

tures such as those based on Graphic Processing Units (GPUs).

In this work, we introduce a novel variational phase-space method for open quantum bosonic systems, based on an analytical Variational Multi-Gaussian (VMG) ansatz for the Wigner function (see Fig. 1). Our approach achieves accuracies comparable to exact diagonalization while maintaining exceptional scalability. The ansatz consists of a sum of Gaussian components, whose number can be systematically increased to control the precision of the solution. The time evolution of the variational parameters is derived analytically and exactly using the Dirac–Frenkel variational principle, exploiting the phase-space functional representation, the analytical properties of multi-Gaussian functions and fully leveraging automatic differentiation [37, 38].

The paper is organized as follows. In Section I, we outline the phase-space framework used to describe the open quantum bosonic systems. Section II introduces the Variational Multi-Gaussian (VMG) ansatz, while in Section III we derive the equations for the time-dependent variational parameters from the Dirac–Frenkel variational principle. In Section IV, we show how this ansatz is particularly well-suited for implementation via automatic differentiation, enabling efficient and scalable simulations. In Section V, we benchmark the method on a single driven-dissipative Kerr quantum parametric oscillator, comparing both the time evolution of observables and the Wigner function to exact results. This test case highlights the method’s ability to capture with exquisite precision highly non-Gaussian features, including pronounced Wigner negativities. In Section VI, we apply our framework to a two-dimensional driven-dissipative Bose–Hubbard lattice with two-boson coherent driving and losses, focusing on the steady-state properties. We successfully benchmark against steady-state results from the literature while extending simulations to significantly larger system sizes. In Section VII, we demonstrate that our approach accurately captures the critical quantum dynamics and provides the first calculation of the dynamical critical exponent associated with the corresponding second-order phase transition. Conclusions and perspectives are presented in Section VIII.

I. PHASE-SPACE REPRESENTATION OF THE OPEN QUANTUM MANY-BOSON DYNAMICS

A. Open quantum dynamics in phase space

The dynamics of the density matrix $\hat{\rho}$ of an open quantum bosonic system, in the presence of weak coupling to a Markovian environment, is described by the Lindblad master equation [39]:

$$\frac{\partial \hat{\rho}(t)}{\partial t} = \mathcal{L}\hat{\rho}(t) = -i[\hat{H}, \hat{\rho}(t)] + \sum_j \mathcal{D}_j[\hat{\rho}(t)]. \quad (1)$$

In this master equation, \mathcal{L} stands for the Liouvillian superoperator which depends on the system’s Hamiltonian \hat{H} which, in turn, encodes the unitary evolution of the system. The dissipation superoperators \mathcal{D}_j account instead for the interaction channels with the external environment, whose action on the density matrix $\hat{\rho}$ is fully characterized by the jump operators $\hat{\Gamma}_j$:

$$\mathcal{D}_j\hat{\rho}(t) = \hat{\Gamma}_j\hat{\rho}(t)\hat{\Gamma}_j^\dagger - \frac{1}{2}\{\hat{\Gamma}_j^\dagger\hat{\Gamma}_j, \hat{\rho}(t)\}. \quad (2)$$

All terms in the Lindblad master equation in Eq. (1) can be expressed in terms of the bosonic annihilation and creation operators, $\hat{\mathbf{a}} = (\hat{a}_1, \hat{a}_2, \dots, \hat{a}_M)$ and $\hat{\mathbf{a}}^\dagger = (\hat{a}_1^\dagger, \hat{a}_2^\dagger, \dots, \hat{a}_M^\dagger)$, corresponding to the M modes of the system. These obey the standard commutation relations $[\hat{a}_j, \hat{a}_k^\dagger] = \delta_{jk}$, and $[\hat{a}_j, \hat{a}_k] = [\hat{a}_j^\dagger, \hat{a}_k^\dagger] = 0$.

The representation of a quantum system as a density matrix $\hat{\rho}$ is not the unique option. By analogy to classical statistical mechanics, one can show that the same information can be stored in a phase-space distribution [40]. In this framework, the density matrix $\hat{\rho}$ is represented by a normalized quasi-probability density function $W(\mathbf{q}, \mathbf{p})$, known as the Wigner function, where $\mathbf{q} = (q_1, q_2, \dots, q_M)$ and $\mathbf{p} = (p_1, p_2, \dots, p_M)$ are the phase-space real quadratures and M is the total number of bosonic modes. The designation *quasi*-probability reflects that, in stark contrast to classical probability density functions, the Wigner function might assume negative values. Note that there are other possible valid phase-space representations of the density matrix, most notably the Glauber–Sudarshan P [41, 42] and the Husimi Q [43], which will not be considered in this work.

The Wigner function on the phase-space variables (\mathbf{q}, \mathbf{p}) is defined in terms of the density matrix $\hat{\rho}$ [40]:

$$W(\mathbf{q}, \mathbf{p}) = \frac{1}{(\pi\hbar)^M} \int_{-\infty}^{+\infty} d\mathbf{y} \langle \mathbf{q} - \mathbf{y} | \hat{\rho} | \mathbf{q} + \mathbf{y} \rangle e^{2i\mathbf{p}\cdot\mathbf{y}/\hbar}. \quad (3)$$

Besides providing an alternative formulation of quantum mechanics, this phase-space formulation recasts quantum mechanics from its usual operator-based (algebraic) picture into a differential one. In this formulation, quantum operators acting on the density matrix are replaced by polynomials and derivatives, defined on the phase-space domain, which act on the Wigner function. The transformation acting on the quantum state $\hat{\rho}$ in Eq. (3) also maps the “algebraic” Liouvillian operator \mathcal{L} to a differential one, \mathcal{L}_W , whose structure is expressed in detail in the Appendix B. In phase-space, the dynamics of the density matrix in Eq. (1) can be recast as:

$$\frac{\partial W(\mathbf{q}, \mathbf{p}, t)}{\partial t} = \mathcal{L}_W W(t) = \{H_W, W(t)\}_{MB} + \sum_j \gamma_j \mathcal{D}_{Wj}[W(t)], \quad (4)$$

where $\{\circ, \circ\}_{MB}$ and \mathcal{D}_W are, respectively, the Moyal brackets and the phase-space dissipation superoperator, both defined in detail in the Appendix B.

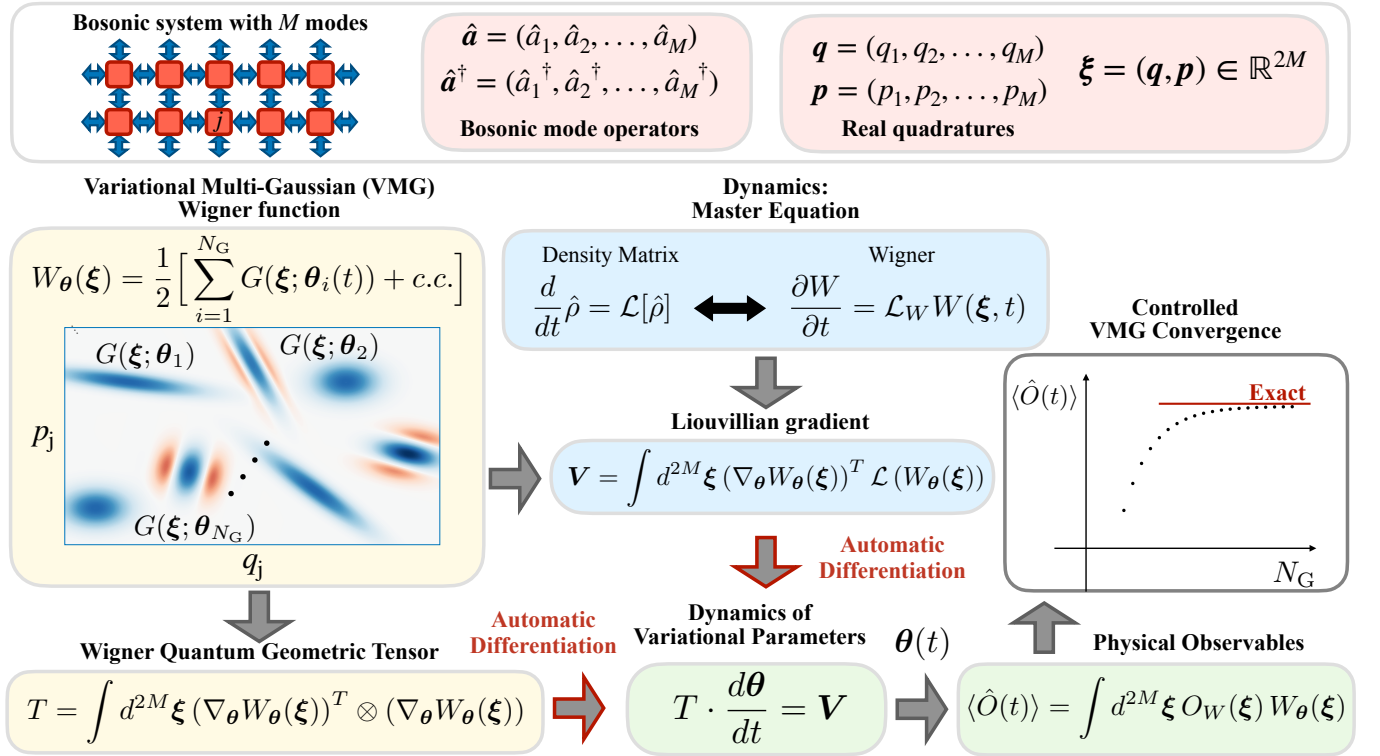


FIG. 1. Scheme of the variational method demonstrated in this work to calculate accurately the dynamics of a quantum system consisting of M bosonic modes. The ansatz for the Wigner function W_θ , representing the many-boson density matrix $\hat{\rho}$, is expressed as a sum of N_G Gaussian functions (and their complex conjugates *c.c.*) each characterized by its variational parameters θ_i : a normalization factor, the center of the Gaussian and its covariance matrix. The Wigner function is defined with respect to the variable $\xi = (q, p)$ where the vectors $q = (q_1, q_2, \dots, q_M)$ and $p = (p_1, p_2, \dots, p_M)$ contain the real quadrature variables describing the M bosonic modes. Since the centers can be complex, the resulting (squeezed) Gaussians are modulated by sinusoidal functions and can therefore take both positive (shown in blue) and negative (shown in red) values. The time evolution of the variational parameter vector θ is governed by the Lindblad master equation (Eq. (1)) through the Dirac-Frenkel variational principle. Specifically, the time derivative $d\theta/dt$ of the variational parameters depends on the Wigner-space quantum geometric tensor T and the Liouvillian gradient vector \mathbf{V} . Both quantities are determined by multidimensional phase-space integrals, which can be computed exactly due to the analytical properties of Gaussian functions and efficiently using automatic differentiation techniques. Any time-dependent observable $\hat{O}(t)$ can be evaluated efficiently via the analytical integral of its Weyl symbol O_W over the Wigner function at time t . The VMG ansatz ensures controlled convergence toward the exact solution by increasing the number N_G of Gaussian functions.

The fact that the phase-space formulation of quantum mechanics is based on the application of differential operators rather than algebraic linear operators makes it suitable for the application of automatic differentiation. This computational technique is designed to automatically calculate partial derivatives [44] and has improved dramatically in recent years due to its applications to machine learning and artificial intelligence.

II. VARIATIONAL MULTI-GAUSSIAN ANSATZ FOR WIGNER FUNCTION

In this work, we adopt a variational approach in which we consider an ansatz for the Wigner function consisting

of a sum of N_G Gaussian functions, namely:

$$W_\theta(\xi) = \frac{1}{2} \left(\sum_{i=1}^{N_G} G(\xi; \theta_i) + c.c. \right) \equiv \sum_{i=1}^{N_G} \text{Re}[G(\xi; \theta_i)], \quad (5)$$

where *c.c.* stands for the complex conjugate and $\theta = (\theta_1, \theta_2, \dots, \theta_{N_G})$ is the vector of variational parameters. Each Gaussian function of the multi-mode phase-space variables $\xi = (q, p)$ is defined as [45, 46]

$$G(\xi; \theta_i) = \frac{c_i}{\sqrt{(2\pi)^M \det(\Sigma_i)}} \exp \left[-\frac{1}{2} (\xi - \mu_i) \Sigma_i^{-1} (\xi - \mu_i) \right], \quad (6)$$

where $\theta_i = (c_i, \mu_i, \Sigma_i)$ is the parameter vector including the variational parameters of the i -th Gaussian, namely the normalization coefficient c_i , the center μ_i and the covariance matrix Σ_i . Note that the normalization also

depends on M , namely the number of bosonic modes. In order for an ensemble of Gaussians to be expressive enough to capture Wigner functions with negative fringes due to macroscopic quantum interference (such as those present for the so-called “Schrodinger cat states” [47, 48]), we allow the centers $\boldsymbol{\mu}$ to take complex values: $\boldsymbol{\mu} = \boldsymbol{\alpha} + i\boldsymbol{\beta}$, where i is the imaginary unit. The real part of a complex-centered Gaussian corresponds in fact to a Gaussian envelope modulated by a sinusoidal function. This form has been shown to exactly reproduce the negative fringes of cat states [45, 49, 50]. The condition that the density matrix has trace equal to one ($\text{Tr}[\hat{\rho}] = 1$) requires the condition for the normalization factors:

$$\sum_{i=1}^{N_G} c_i = 1, \quad c_i \geq 0 \text{ for all } i. \quad (7)$$

Moreover, in our ansatz we will require the Hermitian covariance matrices Σ_i to be real and semi-definite positive. Note that there is not a unique way to parametrize the covariance matrices $\Sigma(\boldsymbol{\theta})$ as functions of the variational parameters $\boldsymbol{\theta}$. We discuss in detail the choice for our variational parameters in Appendix D. An alternative ansatz, based on linear superposition of gaussian states for individual quantum trajectories, has also been recently proposed [51]. Their stochastic method has been exploited to investigate dynamical effects for a Kondo model.

The considered variational multi-Gaussian ansatz, reported in Eq. (5), offers a controllable level of expressivity: the accuracy of the description for arbitrary observables can be systematically improved by increasing the number of Gaussian components. Moreover, the Gaussian structure enables an efficient and fully analytical derivation of the equations governing the time evolution of the variational parameters.

In fact, to compute the time evolution of this ansatz Wigner function $W_{\boldsymbol{\theta}}$, we take advantage of recent advances in automatic differentiation [52, 53]. The use of automatic differentiation is made possible by the fact that the action of any operator on the Wigner function is that of a polynomial in the phase-space variables $\boldsymbol{\xi}$ and in its derivatives $\partial_{\boldsymbol{\xi}}$. As detailed in the following, these polynomials can be computed by means of repeated applications of partial derivatives, which can be automatically and efficiently computed via automatic differentiation.

III. DYNAMICAL EQUATIONS OF OPTIMAL VARIATIONAL PARAMETERS

In order to determine the dynamics of an open bosonic quantum system using the Variational Multi-Gaussian ansatz for the Wigner function, we apply the time-dependent Dirac–Frenkel variational principle [54]. This yields the equations governing the evolution of the optimal variational parameters. Considering a variational

ansatz $\hat{\rho}_{\boldsymbol{\theta}(t)}$ for the density matrix, the corresponding differential equations for the variational parameters read:

$$T \cdot \frac{d}{dt} \boldsymbol{\theta} = \mathbf{V}, \quad (8)$$

where

$$\begin{aligned} T_{rs} &= \text{Tr}[(\nabla_{\boldsymbol{\theta}} \hat{\rho}_{\boldsymbol{\theta}})^\dagger_r (\nabla_{\boldsymbol{\theta}} \hat{\rho}_{\boldsymbol{\theta}})_s], \\ V_r &= \text{Tr}[(\nabla_{\boldsymbol{\theta}} \hat{\rho}_{\boldsymbol{\theta}})^\dagger_r \hat{\mathcal{L}} \hat{\rho}]. \end{aligned} \quad (9)$$

Here, T_{rs} is the quantum geometric tensor, which is solely determined by the structure of the variational ansatz. The vector V_r represents instead the Liouvillian gradient, which depends both on the structure of the variational ansatz and on the form of the master equation governing the system’s dynamics.

In the Wigner representation these quantities can be expressed as phase-space integrals, namely:

$$\begin{aligned} T &= \int d^{2M} \boldsymbol{\xi} \left(\nabla_{\boldsymbol{\theta}} W_{\boldsymbol{\theta}}(\boldsymbol{\xi}) \right)^T \otimes \left(\nabla_{\boldsymbol{\theta}} W_{\boldsymbol{\theta}}(\boldsymbol{\xi}) \right), \\ \mathbf{V} &= \int d^{2M} \boldsymbol{\xi} \left(\nabla_{\boldsymbol{\theta}} W_{\boldsymbol{\theta}}(\boldsymbol{\xi}) \right)^T \mathcal{L}_W(W_{\boldsymbol{\theta}}(\boldsymbol{\xi})), \end{aligned} \quad (10)$$

where $d^{2M} \boldsymbol{\xi} = d^M \mathbf{q} d^M \mathbf{p}$.

IV. EFFICIENT GENERALIZED GAUSSIAN MOMENTS VIA AUTOMATIC DIFFERENTIATION

A central challenge for time-dependent variational methods is to design an ansatz that is both highly expressive and enables an efficient evaluation of the quantum geometric tensor and the Liouvillian gradient. As we demonstrate below, our variational approach based on automatic differentiation successfully meets both requirements and opens the door to remarkable applications that have remained out of reach for existing methods.

Quantum states in the Variational Multi-Gaussian form are especially amenable to analytical treatment for their variational dynamical evolution. Specifically, for a VMG Wigner function $W_{\boldsymbol{\theta}}$ as in Eq. (5), the Wigner quantum geometric tensor T can be conveniently computed by taking the gradients $\nabla_{\boldsymbol{\theta}}$ outside the sign of the integral in Eq. (10). Namely, we get the expression:

$$\begin{aligned} T[\boldsymbol{\theta}] &= \sum_{m,n=1}^{N_G} \nabla_{\boldsymbol{\theta}} \nabla_{\boldsymbol{\theta}'} \int d^{2M} \boldsymbol{\xi} \times \\ &\quad \text{Re}[G(\boldsymbol{\xi}; \boldsymbol{\theta})] \text{Re}[G(\boldsymbol{\xi}; \boldsymbol{\theta}')] \Big|_{\substack{\boldsymbol{\theta}=\boldsymbol{\theta}_m \\ \boldsymbol{\theta}'=\boldsymbol{\theta}_n}}. \end{aligned} \quad (11)$$

In an analogous fashion, the Liouvillian gradient \mathbf{V} in Eq. (10) can be recast as:

$$\begin{aligned} V[\boldsymbol{\theta}] &= \sum_{m,n=1}^{N_G} \nabla_{\boldsymbol{\theta}} \int d^{2M} \boldsymbol{\xi} \times \\ &\quad \text{Re}[G(\boldsymbol{\xi}; \boldsymbol{\theta})] \mathcal{L}_W \text{Re}[G(\boldsymbol{\xi}; \boldsymbol{\theta}')] \Big|_{\substack{\boldsymbol{\theta}=\boldsymbol{\theta}_m \\ \boldsymbol{\theta}'=\boldsymbol{\theta}_n}}. \end{aligned} \quad (12)$$

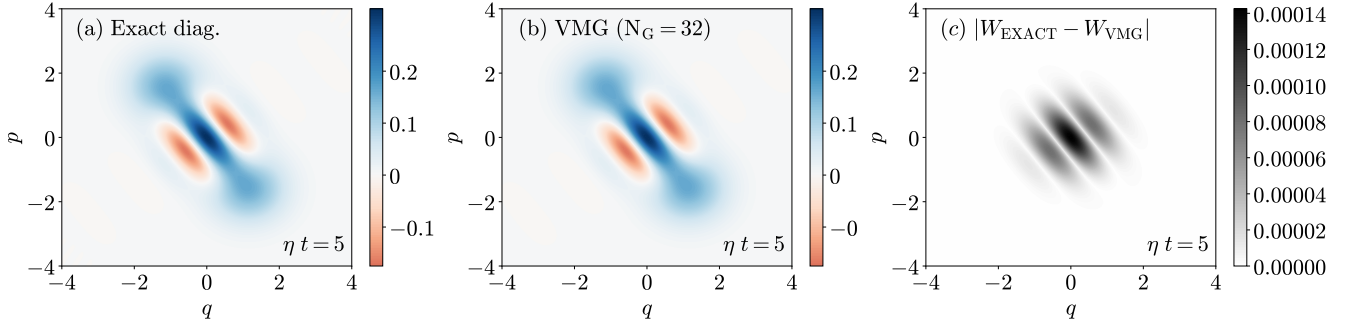


FIG. 2. (a) Wigner function at time $t = 5/\eta$ obtained via exact diagonalization techniques (specifically via Fock base expansion with bosonic cutoff $\Lambda_b = 100$) for the single-mode dissipative Kerr parametric oscillator. The non-unitary dynamics is governed by the Hamiltonian described by Eq. (16) (boson-boson interaction with two-boson driving) and by two-boson loss rate η . The system is initially in the vacuum state at time $t = 0$. (b) Wigner function at the same time computed using the Variational Multi-Gaussian (VMG) ansatz with 32 complex Gaussians. (c) Absolute value of the difference between the exact and the variational Wigner functions, highlighting the remarkable accuracy of the VMG ansatz, which, unlike the exact integration approach, is scalable to systems with many modes. Other parameters: boson-boson interaction $U/\eta = 1$, single-boson loss-rate $\gamma = 0$, detuning $\Delta = 0$ and two-boson driving complex amplitude $G/\eta = 3 + 3i$.

Here, the gradient $\nabla_{\boldsymbol{\theta}}$ can be taken outside of the integral because it applies only to the first term ($\text{Re}[G(\boldsymbol{\xi}; \boldsymbol{\theta})]$), while it is zero on the second ($\mathcal{L}_W \text{Re}[G(\boldsymbol{\xi}; \boldsymbol{\theta}')]$). As detailed in Appendix B 1, the Liouvillian operator \mathcal{L} can be decomposed as $\mathcal{L}_W = \sum_{\mathbf{I}} \mathcal{L}_{W, \mathbf{I}}$, where each Liouvillian component is such that:

$$\mathcal{L}_{W, \mathbf{I}} \propto \xi_{i_1} \dots \xi_{i_l} \partial_{\xi_{j_1}} \dots \partial_{\xi_{j_k}}. \quad (13)$$

This means that, in order to compute the Liouvillian gradient vector \mathbf{V} , we need to evaluate the *generalized Gaussian moments* defined as follows:

$$\langle \xi_{i_1} \dots \xi_{i_l} \partial_{\xi_{j_1}} \dots \partial_{\xi_{j_k}} \rangle_{\boldsymbol{\theta}, \boldsymbol{\theta}'} = \int d^{2M} \boldsymbol{\xi} \times \text{Re}[G(\boldsymbol{\xi}; \boldsymbol{\theta})] \xi_{i_1} \dots \xi_{i_l} \partial_{\xi_{j_1}} \dots \partial_{\xi_{j_k}} \text{Re}[G(\boldsymbol{\xi}; \boldsymbol{\theta}')]. \quad (14)$$

The Eq. (14), for the generalized Gaussian moments, can be streamlined by recasting them as derivatives with respect to vanishing currents \mathbf{J} and $\tilde{\mathbf{J}}$ of a generating function $\mathcal{Z}[\mathbf{J}, \tilde{\mathbf{J}}]$:

$$\langle \xi_{i_1} \dots \xi_{i_l} \partial_{\xi_{j_1}} \dots \partial_{\xi_{j_k}} \rangle_{\boldsymbol{\theta}, \boldsymbol{\theta}'} = \partial_{J_{i_1}} \dots \partial_{J_{i_l}} \partial_{\tilde{J}_{j_1}} \dots \partial_{\tilde{J}_{j_k}} \mathcal{Z}[\mathbf{J}, \tilde{\mathbf{J}}] |_{\mathbf{J}=0, \tilde{\mathbf{J}}=0}. \quad (15)$$

The functional form of the generating function $\mathcal{Z}[\mathbf{J}, \tilde{\mathbf{J}}]$ is reported in Appendix A, along with the method to obtain it. In this framework, the matrix $T[\boldsymbol{\theta}]$ and the vector $V[\boldsymbol{\theta}]$ are thus analytically computed via automatic differentiation.

The ability to simulate the dynamics of a two-dimensional Bose-Hubbard system with two-boson coherent driving and two-body losses in the quantum critical regime for large lattice sizes highlights the unprecedented efficiency of our phase-space method. The key breakthrough behind its accuracy and scalability lies in the full exploitation of the analytical properties of Gaussian functions through generalized Gaussian moments,

combined with the use of state-of-the-art automatic differentiation and Taylor-mode expansion tailored to our physical setting. In contrast, previous approaches based on Gaussian ansätze in phase space [55] were severely limited in both accuracy and scalability due to their reliance on purely numerical variational minimization, which neglected the analytical structure of Gaussian functions and did not leverage automatic differentiation—both of which are crucial for treating systems with a large number of modes.

Automatic differentiation provides a systematic framework for computing partial derivatives [44], and has seen rapid advancements in recent years, driven by its central role in machine learning and artificial intelligence. In the present context, we had the idea of exploiting this novel technique from computer science to evaluate analytically and automatically the generalized Gaussian moments associated with the Liouvillian operator \mathcal{L} , which fully determine the equations of motion for the variational parameters $\boldsymbol{\theta}$. Note that computing high-order moments via nested automatic differentiation poses significant memory challenges, which increases exponentially with the order of derivatives. As shown in Appendix B, for an Hamiltonian whose terms are at most of quartic order in the bosonic operators and for Lindblad jump operators that are at most quadratic in the bosonic operator, we have to deal at most with derivatives of order 4. Moreover, the addition of the gradient with respect to the variational parameters $\boldsymbol{\theta}$ in Eq. (12) increases, this maximal order of derivative, to the order 6. To address this technical challenge, we have employed Taylor-mode automatic differentiation [56], a mathematically efficient—though still underutilized—technique [57] based on expanding functions into their Taylor series. This approach achieves at least factorial improvements in computational efficiency with respect to standard automatic differentiation, particularly with high-order deriva-

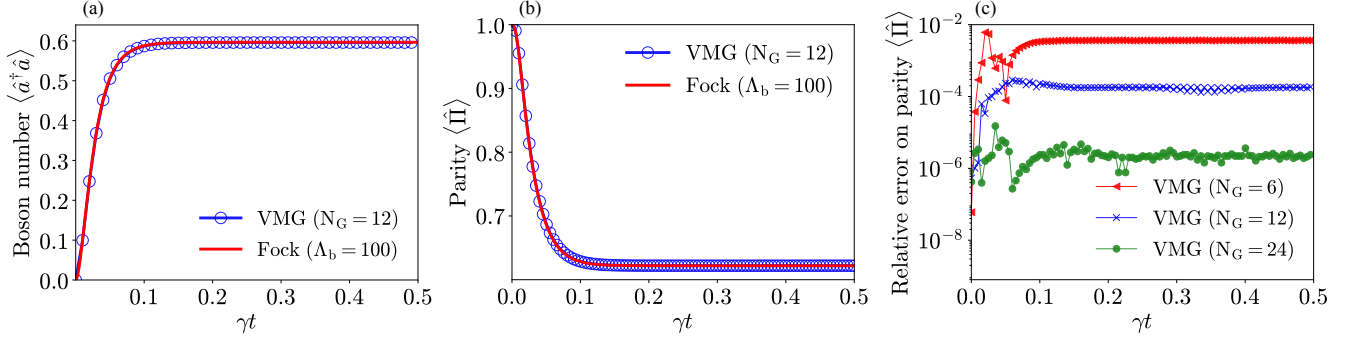


FIG. 3. Dynamics of observables for the same open quantum system as in Fig. 2, but with a different set of illustrative parameters. (a) Time evolution of the boson occupation number. The exact solution (solid red line) is compared to the VMG result (solid blue with marker) obtained with 12 complex Gaussians. (b) Same as in (a), but for the parity expectation value. (c) Relative error (in log scale) of the dynamics of the parity expectation value. This relative error decreases *exponentially* with the number of Gaussians used in the VMG ansatz. The initial state is the vacuum. Parameters: $U/\gamma = \Delta/\gamma = 0.1$, $\eta = 0$, $G/\gamma = 0.3 + 0.3i$.

tives. By extracting the relevant Taylor coefficients, the required derivatives are obtained directly and simultaneously, making this method especially well-suited for the memory- and time-efficient computation of higher-order generalized Gaussian moments [38]. In this work, we compute all such moments governing the dynamics in Eq. (12) using Taylor-mode automatic differentiation as implemented in the `jax.experimental.jet` module of the JAX framework [53]. Specifically, we employ Taylor mode automatic differentiation to compute the derivatives with respect to the vanishing currents \mathbf{J} and $\hat{\mathbf{J}}$ in Eq. (14), while we adopt standard automatic differentiation with respect to the variational parameters θ in the computation of the quantum geometric tensor T and Liouvillian gradient V in Eqs. (11) and (12) respectively.

V. SINGLE KERR PARAMETRIC OSCILLATOR

In order to benchmark our variational dynamical approach, we start by considering a bosonic system consisting of a single mode, where exact diagonalization can be performed. In particular, we study the Kerr parametric quantum oscillator, where bosonic Schrödinger cat states can emerge during the dynamics. This quantum model lies at the heart of several photonic quantum computing platforms [7, 14–16, 58]. We explore the oscillator’s dynamics across a broad range of parameter regimes, including the deep quantum regime in which the Wigner function displays negative fringes. Notably, these regions are beyond the reach of conventional phase-space techniques such as the truncated Wigner approximation, the positive-P representation, or Gaussian trajectory methods [36]. In the reference frame rotating at half the pump frequency ($\hbar = 1$), the Hamiltonian of a single-site Kerr parametric oscillator reads

$$\hat{H} = \frac{U}{2} \hat{a}^{\dagger 2} \hat{a}^2 + \frac{G}{2} \hat{a}^{\dagger 2} + \frac{G^*}{2} \hat{a}^2 - \Delta \hat{a}^\dagger \hat{a}. \quad (16)$$

Here \hat{a} is the bosonic annihilation operator ($[\hat{a}^\dagger, \hat{a}] = 1$), U is the strength of the Kerr nonlinearity, and G is the two-boson pump driving amplitude. The detuning is defined as $\Delta = \frac{\omega_p}{2} - \omega_c$, where ω_p is the pump frequency and ω_c the cavity frequency. We study the dynamics of the system under single- and two-boson losses, occurring at rates γ and η , respectively. The corresponding jump operators are $\hat{\Gamma}_1 = \sqrt{\gamma} \hat{a}$ and $\hat{\Gamma}_2 = \sqrt{\eta} \hat{a}^2$. For the single-mode case, we employed a brute-force exact diagonalization procedure using a Fock basis with a cutoff Λ_b on the maximum number of bosons. Simulations were performed using the open-source software QuTip [59], and convergence was carefully checked by increasing the cutoff.

Note that, in the steady state, the Wigner function for a Kerr parametric oscillator is always positive [60]. Nevertheless, the Wigner function, in a regime with a small single-boson loss rate $\gamma/\eta \ll 1$, can display regions with deep Wigner negativities during the temporal transient. As shown in Fig. 2(a), realized for $\gamma = 0$, the time evolution of the Wigner function, reconstructed via exact diagonalization (Fock cutoff $\Lambda_b = 100$), displays negative values. This snapshot of the Wigner function is realized at time $\eta t = 5$, i.e. well before the system has relaxed to the steady state. As it can be seen in Fig. 2(b)-(c), a VMG ansatz with 32 complex Gaussian functions excellently reproduces the dynamics of the Wigner function in a regime where it is highly non-Gaussian and with deep negativities. Panels (a) and (b) are not distinguishable by eye. Panel (c) displays the negligible difference on a color-scale reduced by several orders of magnitude. With the Wigner function, every observable can be computed. As explained in Appendix B, this is achieved analytically by integrating the corresponding Weyl symbols O_W of the observables over the Multi-Gaussian Wigner function $W_\theta(\xi)$ for any time t .

Specifically, in Fig. 3(a)-(b) we report the time evolution of both the boson number $\hat{N} \equiv \hat{a}^\dagger \hat{a}$ and the parity

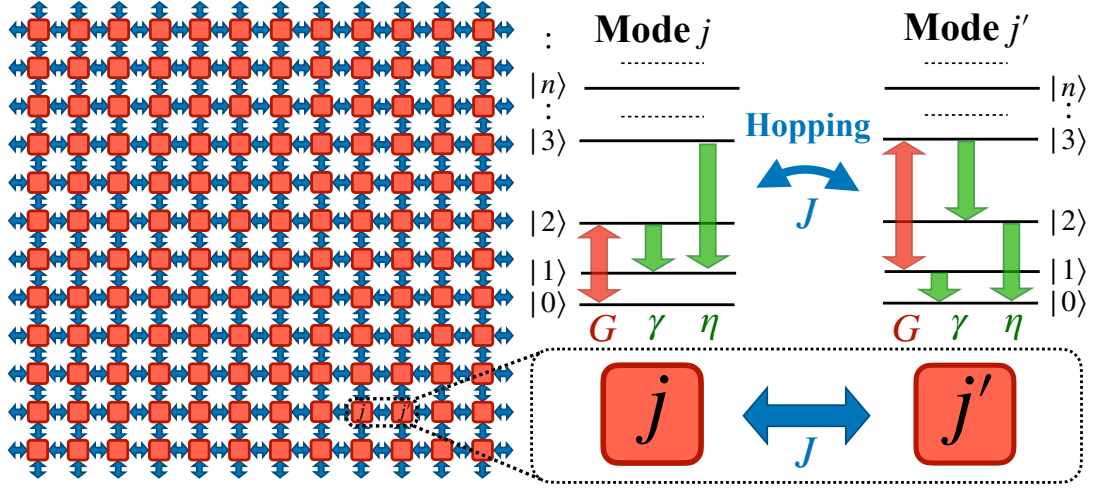


FIG. 4. Scheme of the considered 12×12 Bose-Hubbard lattice system with periodic boundary conditions with two-boson driving and losses. The term G stands for the two-boson driving amplitude, while γ and η represent the single- and two-boson loss rates respectively. Nearest-neighbor sites (modes) are coupled by the boson hopping quantified by J . The energy levels of the Fock states of each mode are not equally spaced reflecting the presence of the on-site boson-boson interaction U .

operator $\hat{\Pi} \equiv \exp(i\pi\hat{a}^\dagger\hat{a})$. For this given Hamiltonian, already for a small number of Gaussians in the ansatz, such as $N_G = 6$, the agreement with the exact dynamics is outstanding. Remarkably, the relative error on the observables can be exponentially reduced by increasing the number of Gaussian functions N_G in Eq. (5), as shown with a log scale in Fig. 3(c). In particular, by increasing the number of Gaussians by a factor 4, the relative error decreases by approximately 4 orders of magnitudes.

VI. BOSE-HUBBARD LATTICES WITH TWO-BOSON DRIVING AND DISSIPATION

In this Section, we will consider a nontrivial system: the Bose-Hubbard model with periodic boundary conditions subject to two-boson coherent driving, as well as both single-boson and two-boson losses. This system, pictured in Fig. 4, can be viewed as a lattice of Kerr parametric quantum oscillators, with each site coupled to its nearest neighbors via hopping. In the previous section, we have considered the system consisting of a single site.

Networks of coupled Kerr parametric oscillators have garnered significant attention due to their ability to form interacting lattices, offering a promising platform for quantum information processing [64]. In particular, these systems—alongside optical parametric oscillators [65]—have been proposed as hardware-efficient solvers for the Ising problem and as intrinsically noise-resilient architectures for quantum computation [5]. The Hamiltonian of the

corresponding model reads ($\hbar = 1$)

$$\hat{H} = \sum_{j=1}^M \left[-\Delta \hat{a}_j^\dagger \hat{a}_j + \frac{U}{2} \hat{a}_j^{\dagger 2} \hat{a}_j^2 + \frac{G}{2} \hat{a}_j^{\dagger 2} + \frac{G^*}{2} \hat{a}_j^2 \right] - \sum_{\langle j,j' \rangle} \frac{J}{z} (\hat{a}_j^\dagger \hat{a}_{j'} + \hat{a}_j \hat{a}_{j'}^\dagger), \quad (17)$$

where \hat{a}_j denotes the bosonic annihilation operator of the j -th mode (site), U is the Kerr nonlinearity, Δ the detuning, G the two-boson drive amplitude, and J the nearest-neighbor hopping rate normalized by the coordination number z . Single- and two-boson losses are incorporated via the dissipation superoperator \mathcal{D} acting on the density matrix $\hat{\rho}(t)$:

$$\mathcal{D}[\hat{\rho}(t)] = \sum_{k=1}^2 \sum_{j=1}^M \left[\hat{\Gamma}_{k,j} \hat{\rho}(t) \hat{\Gamma}_{k,j}^\dagger - \frac{1}{2} \{ \hat{\Gamma}_{k,j}^\dagger \hat{\Gamma}_{k,j}, \hat{\rho}(t) \} \right], \quad (18)$$

where M denotes the number of lattice sites, and the jump operators on site j are given by

$$\hat{\Gamma}_{1,j} = \sqrt{\gamma} \hat{a}_j \quad \text{and} \quad \hat{\Gamma}_{2,j} = \sqrt{\eta} \hat{a}_j^2, \quad (19)$$

corresponding respectively to single- and two-boson loss processes.

To the best of our knowledge, a finite-size scaling analysis of this model has been studied only in the steady state [24], using the Corner Space Renormalization method [23], which is a technique to find the stationary states of low-entropy open quantum systems where the basis of states is judiciously constructed through a spatial renormalization procedure. The Corner Space Renormalization has controllable accuracy, as in exact diagonalization approaches, and the lattice size that can

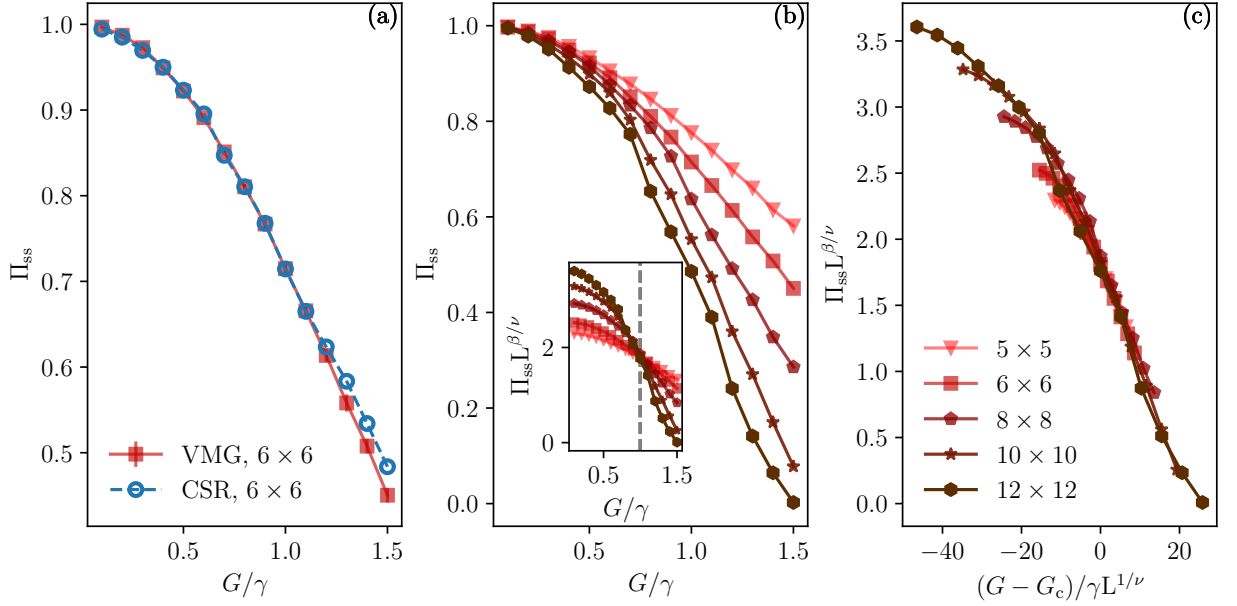


FIG. 5. (a) Comparison between the steady-state expectation value of the global parity operator obtained using both the Corner Space Renormalization method (CSR) [24] and our variational approach with a Variational Multi-Gaussian (VMG) ansatz, employing $N_G = 16$ Gaussians for a 2D driven-dissipative Bose-Hubbard lattice Eq. (17). (b) Steady-state parity expectation values computed with our variational approach ($N_G = 16$) for increasing values of L , where $L \times L$ is the number of lattice sites. The parity is plotted as a function of the driving amplitude G/γ . In the inset, the critical pump amplitude G_c (dashed vertical line) is estimated to be at $G_c \approx 1.0\gamma$. (c) Rescaled steady-state expectation values of the parity operator as a function of the rescaled pump amplitude. The critical exponents β and ν employed are those of the 2D quantum Ising model in a transverse field: $\beta = 0.32641871$, $\nu = 0.62997097$ [61–63]. The critical value of the two-boson pump amplitude is $G_c \approx 1.0\gamma$. Parameters: $\Delta/\gamma = -20.0$, $\eta/\gamma = 1.0$, $U/\gamma = 40.0$, and $J/\gamma = 20.0$.

be simulated is limited by the memory of the calculated density matrix, which depends on its entropy. Here, we will benchmark our predictions for the steady-state observables against the results obtained with the Corner Space Renormalization method [24], and we will extend the analysis to much larger lattice sizes. In the next section, we investigate the critical dynamics of this system, which—to the best of our knowledge—have never been reported by any method in the literature.

The Liouvillian of the considered system, with Hamiltonian in Eq. (17) and dissipator in Eq. (18), is invariant under the transformation $\hat{a}_j \rightarrow -\hat{a}_j$ and $\hat{a}_j^\dagger \rightarrow -\hat{a}_j^\dagger$. This means that the even parity of a Wigner function in phase space $W(\mathbf{q}, \mathbf{p}) = W(-\mathbf{q}, -\mathbf{p})$ is preserved by the time evolution described by the master equation. Such non-equilibrium Bose-Hubbard model undergoes a dissipative quantum phase transition [24] for a critical value of the two-boson driving amplitude G , associated with a spontaneous symmetry breaking of such discrete \mathbb{Z}_2 symmetry of the Liouvillian in the thermodynamical limit.

A relevant quantity to characterize this phase transition is the boson number parity operator defined as:

$$\hat{\Pi} = \exp \left(i\pi \sum_{j=1}^M \hat{a}_j^\dagger \hat{a}_j \right). \quad (20)$$

The emergence of the above mentioned phase transition

with increasing lattice size can be witnessed by the finite-size scaling of the expectation value of this parity operator in the steady state [24]. As detailed in Appendix B the expectation value of the parity operator is proportional to the value of the Wigner function at the origin of the phase space. Indeed, as illustrated in Fig. 5, our variational method faithfully reproduces the steady-state parity across the second-order phase transition. In particular, we have achieved an excellent agreement between our results and those obtained via Corner Space Renormalization. As an illustrative example of the successful benchmarking, we report the results for a 6×6 lattice in Fig. 5(a), where we plot the steady-state expectation value of the parity operator versus the driving G .

In Fig. 5(b), we report the parity expectation value versus the two-boson driving G for increasing lattice sizes. Our finite size-scaling analysis shows an emergent phase transition belonging to the universality class of the 2D quantum Ising model. Indeed, as shown in Fig. 5(c), a rescaling [66, 67] of the parity expectation value and of the driving G with the system size L and the critical exponents β and ν , all the curves nicely collapse around the critical driving amplitude G_c . As shown in the inset of Fig. 5(b), the value of the critical driving amplitude G_c can be extracted by the crossing point obtained by rescaling only the parity.

As the system size increases, the convergence time cor-

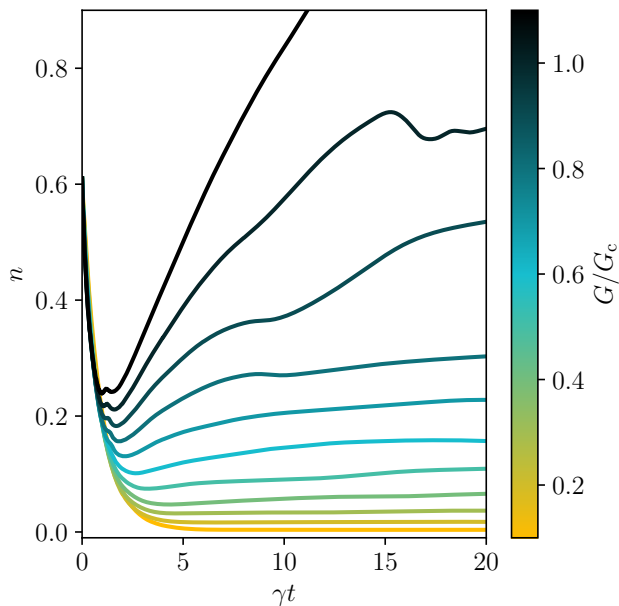


FIG. 6. Time evolution of the average boson number n for a 12×12 Bose-Hubbard lattice. As the drive amplitude G increases, the relaxation dynamics becomes significantly slower. Same parameters as in Fig. 5.

respondingly grows. For the results reported in this work, we evolved the Lindblad master equation up to a final time of $20\gamma^{-1}$, $40\gamma^{-1}$, $60\gamma^{-1}$, $120\gamma^{-1}$, and $120\gamma^{-1}$ for lattice sizes 5×5 , 6×6 , 8×8 , 10×10 , and 12×12 , respectively. Note that the calculations for lattices up to 10×10 were carried out on a single Nvidia A100 GPU, while those for the 12×12 lattice were performed on a single Nvidia H100 GPU.

VII. CRITICAL SLOWING DOWN AND DYNAMICAL CRITICAL EXPONENTS

In this section, we apply our variational method to calculate the dynamical properties of the second-order quantum phase transition in the 2D network of Kerr parametric quantum oscillators introduced in the previous section. The study of critical dynamical quantities is challenging because it requires the ability to obtain highly accurate results on large-scale lattices over diverging time scales. In order to characterize the critical dynamics, we focus here on the asymptotic decay rate. This is the rate at which observables approach their steady-state value in the long-time limit. At the critical point, the asymptotic decay rate is expected to vanish, corresponding to a critical slowing down of relaxation [68]. The asymptotic decay rate is also called the Liouvillian frequency gap, as it can be computed from the spectrum of the Liouvillian superoperator.

To the best of our knowledge, this is the first time the dynamics of such a non-equilibrium phase transition is

explored in the quantum regime. Previous studies in the literature have investigated first-order phase transitions in the semiclassical regime of the Bose-Hubbard model with single-boson driving [69], where the Wigner function remains positive and can be simulated using the truncated Wigner approximation. Another work [70] considered single-Gaussian trajectories to study the driven-dissipative 2D Bose-Hubbard model with two-boson driving, but in a semiclassical regime dominated by single-boson losses (indeed, the extracted critical exponents correspond to the universality class of the classical 2D Ising model).

This critical slowing down of the dynamics for the considered model can be appreciated in Fig. 6, where, for a 12×12 lattice, we show the dynamical evolution of the expectation value of the mean boson number $n = \langle \hat{n} \rangle$:

$$\hat{n} = \frac{1}{L^2} \sum_{j=1}^{L^2} \hat{a}_j^\dagger \hat{a}_j, \quad (21)$$

where L^2 is the number of sites of the square $L \times L$ -lattice. We refer to Appendix D for a detailed description of the initial conditions used for the calculated dynamics.

By examining Fig. 6, one observes that as the two-boson driving amplitude G approaches the critical value G_c , the time required to reach the steady state becomes progressively longer. Specifically, while for $G/G_c \ll 1$ the system relaxes well before time $t = 20\gamma^{-1}$, for $G = G_c$ the dynamics is still far from the steady state after the same time. This diverging time scale highlights how the variational approach captures the vanishing of the gap λ near the critical point G_c . As already mentioned, the relaxation time near the critical driving further increases when increasing the system size, as shown in Fig. 7(a).

In Fig. 7(b), we report the behavior of the Liouvillian gap for different system sizes ranging from 25 to 144 bosonic modes. As expected for second-order phase transitions [68], the gap tends toward vanishingly small values near the critical point, leading to a diverging relaxation time in the thermodynamic limit.

Remarkably, in Fig. 7(c), we demonstrate that the driven-dissipative Bose-Hubbard model belongs to the Ising universality class by rescaling with the corresponding dynamical critical exponent $z = 2.0235$ [71]. Indeed, when we plot the rescaled asymptotic decay rates λL^z as a function of $(G - G_c)L^{1/\nu}/\gamma$, the data collapse onto a single universal curve in the critical region, which features a sharp drop of the decay rates, which for any value $G > G_c$ vanish in the thermodynamic limit.

VIII. CONCLUSIONS AND OUTLOOK

We have introduced a scalable variational method for simulating the dynamics of interacting open quantum bosonic systems deep in the quantum regime. Our approach is based on a multi-dimensional Wigner phase-space representation and employs a Variational Multi-

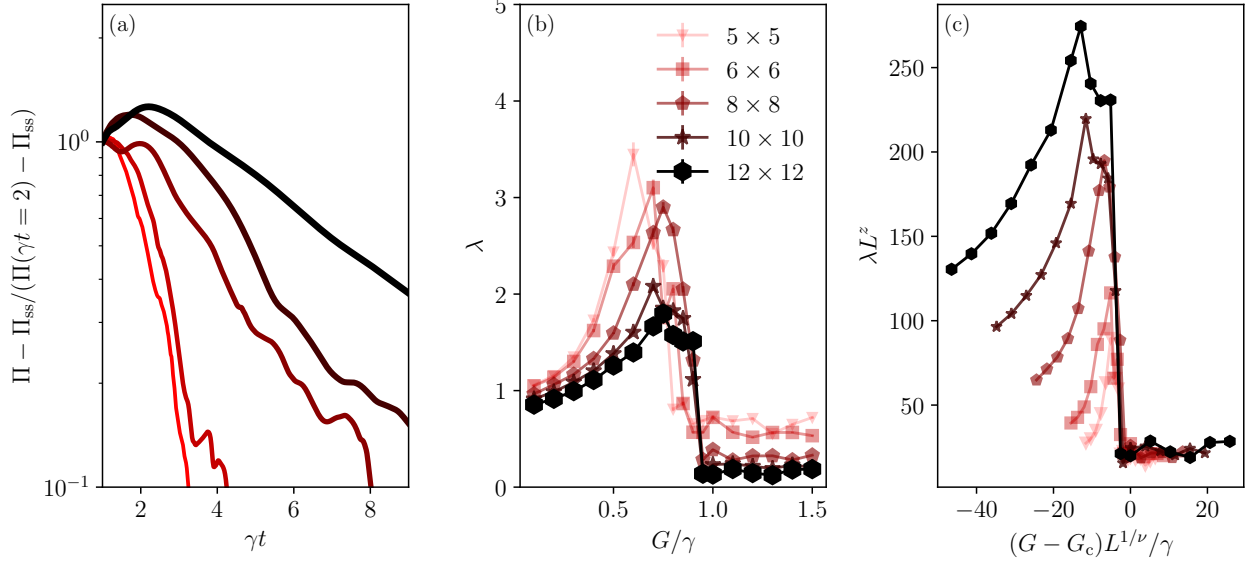


FIG. 7. (a) Illustrative example of the temporal dynamics of the parity operator expectation value, shown on a log scale, at the critical driving amplitude $G = G_c \sim 1.0 \gamma$ for different lattice sizes (see legend in panel b). (b) Asymptotic decay rate λ toward the steady state as a function of the driving amplitude G , shown for different lattice sizes $L \times L$. (c) Finite-size scaling analysis revealing dynamical critical behavior consistent with the 2D quantum Ising universality class, with critical exponent $z = 2.0235$. By rescaling the shifted two-boson driving amplitude $(G - G_c)/\gamma$ with the rescaled lattice side length $L^{1/\nu}$, the rescaled decay rates λL^z collapse onto a single universal curve for all considered system sizes. Same parameters as in Fig. 5.

Gaussian (VMG) ansatz, whose accuracy is systematically controlled by the number of Gaussian components. The equations of motion are derived from the Dirac–Frenkel principle and are evaluated efficiently by leveraging the analytical structure of Gaussian functions together with automatic differentiation.

This framework enables the simulation of dissipative many-body quantum dynamics in strongly correlated regimes, where standard approaches become intractable due to large Hilbert space sizes or strong Wigner negativities. As a key application, we investigated the driven-dissipative two-dimensional Bose–Hubbard model with two-boson coherent driving and two-body losses, accessing its quantum critical dynamics far from equilibrium. By analyzing the time-dependent relaxation and performing finite-size scaling of the Liouvillian spectral gap, we revealed a vanishing asymptotic decay rate and extracted critical exponents belonging to the 2D quantum Ising universality class.

Beyond fundamental insights into strongly interacting bosonic systems, our method provides a powerful computational tool for designing and simulating complex networks of strongly interacting bosonic modes—such as nonlinear quantum oscillators—used in quantum information processing. The ability to model such architectures in the presence of dissipation and strong quantum correlations opens new avenues for the development of ro-

bust quantum technologies. Looking forward, our framework based on automatic differentiation can be extended to other analytical ansätze and to phase-space representations tailored to spins and fermions, enabling broad applications across condensed matter, quantum optics, and quantum engineering.

ACKNOWLEDGMENTS

We acknowledge support from the French ANR project FracTrans (grant ANR-24-CE30-6983) and a grant (Polaritonic) from the French Government managed by the ANR under the France 2030 programme with the reference ANR-24-RR11-0001. This work was granted access to the HPC resources of IDRIS under the allocation 2025-AD010612462R2 made by GENCI. We also gratefully acknowledge the S-CAPAD/DANTE platform, IPGP, France.

Appendix A: Generalized Gaussian moments

As mentioned in the main text, the differential Liouvillian operator \mathcal{L}_W can be decomposed as a sum of multiple terms $\mathcal{L}_{W,\mathbf{I}}$, such that $\mathcal{L} = \sum_{\mathbf{I}} \mathcal{L}_{W,\mathbf{I}}$, all of the form:

$$\mathcal{L}_{W,\mathbf{I}} \propto \xi_{i_1} \dots \xi_{i_l} \partial_{\xi_{j_1}} \dots \partial_{\xi_{j_k}}. \quad (\text{A1})$$

To unravel the time evolution of the variational parameters θ that appear in the variational Wigner function $W_\theta(\xi)$, one needs to compute the Liouvillian gradient vector \mathbf{V} in the equation Eq. (8). When the Wigner function is given by the sum of multiple Gaussian functions, this can be done analytically via automatic differentiation. To simplify the notation, we consider the case of Gaussian functions in which the normalization coefficient $c = 1$ (cf. Eq. (6)). In this case a Gaussian function is identical to the multivariate normal distribution \mathcal{N} with centers μ and covariance matrix Σ : $G(\xi; \theta)|_{c=1} \equiv \mathcal{N}(\xi; \mu, \Sigma)$. The normal distribution is given as:

$$\mathcal{N}(\xi; \mu, \Sigma) = \frac{1}{\sqrt{(2\pi)^M \det(\Sigma)}} \exp\left[-\frac{1}{2}(\xi - \mu)\Sigma^{-1}(\xi - \mu)\right]. \quad (\text{A2})$$

One can start by writing the integral of the terms \mathcal{L}_1 , on a set of normalized Gaussians, in the following fashion:

$$\langle \xi_{i_1} \dots \xi_{i_l} \partial_{\xi_{j_1}} \dots \partial_{\xi_{j_k}} \rangle_{(\mu, \Sigma), (\mu', \Sigma')} \equiv \int d^{2M} \xi \mathcal{N}(\mu, \Sigma) \xi_{i_1} \dots \xi_{i_l} \partial_{\xi_{j_1}} \dots \partial_{\xi_{j_k}} \mathcal{N}(\mu', \Sigma'). \quad (\text{A3})$$

By inserting in the previous equation a source term $e^{\mathbf{J}^T \xi}$ and deriving with respect to \mathbf{J} , the quantity $\xi_{i_1} \dots \xi_{i_k}$ can be factored out of the integral as:

$$\begin{aligned} \int d^{2M} \xi \mathcal{N}(\mu, \Sigma) \xi_{i_1} \dots \xi_{i_l} \partial_{\xi_{j_1}} \dots \partial_{\xi_{j_k}} \mathcal{N}(\mu', \Sigma') = \\ \partial_{J_{i_1}} \dots \partial_{J_{i_l}} \int d^{2M} \xi e^{\mathbf{J}^T \xi} \mathcal{N}(\mu, \Sigma) \times \\ \left. \partial_{\xi_{j_1}} \dots \partial_{\xi_{j_k}} \mathcal{N}(\mu', \Sigma') \right|_{\mathbf{J}=0}. \end{aligned} \quad (\text{A4})$$

Now, let us notice that the term $e^{\mathbf{J}^T \xi} \mathcal{N}(\mu, \Sigma)$, appearing on the left hand side in the previous equation, can be recast as:

$$e^{\mathbf{J}^T \xi} \mathcal{N}(\mu, \Sigma) = e^{\frac{1}{2} \mathbf{J}^T \Sigma \mathbf{J} + \mathbf{J}^T \mu} \mathcal{N}(\mu + \mathbf{J}^T \Sigma, \Sigma). \quad (\text{A5})$$

Not being dependent on any phase-space variable ξ , the factor $e^{\frac{1}{2} \mathbf{J}^T \Sigma \mathbf{J} + \mathbf{J}^T \mu}$ can be safely taken out of the integral in Eq. (A4). Additionally, the term $\partial_{\xi_{j_1}} \dots \partial_{\xi_{j_k}}$, on the right-hand side of Eq. (A4), can be treated analogously to $\xi_{i_1} \dots \xi_{i_l}$ by rewriting the Gaussian function in the Fourier dual space. Specifically the Fourier dual of $\mathcal{N}(\mu, \Sigma)$ is defined as:

$$\mathcal{N}(\mu, \Sigma) = \int d\kappa e^{2\pi i \xi^T \kappa} \tilde{\mathcal{N}}(\mu, \Sigma)[\kappa], \quad (\text{A6})$$

where $\tilde{\mathcal{N}}(\mu, \Sigma)[\kappa]$ explicitly reads as:

$$\tilde{\mathcal{N}}(\mu, \Sigma)[\kappa] = e^{-2\pi i \mu^T \kappa} e^{-2\pi^2 \kappa^T \Sigma \kappa}. \quad (\text{A7})$$

Under such transformation, and introducing for simplicity the notation $\nu = \mu + \mathbf{J}^T \Sigma$, the integrand on the right-hand side of Eq. (A4) becomes:

$$\begin{aligned} \int d^{2M} \xi \mathcal{N}(\nu, \Sigma) \partial_{\xi_{j_1}} \dots \partial_{\xi_{j_k}} \mathcal{N}(\mu', \Sigma') = \\ \int d\xi d\kappa' d\kappa e^{2\pi i \xi^T (\kappa + \kappa')} \tilde{G}(\nu, \Sigma)[\kappa'] \times \\ (2\pi i)^n \kappa_{j_1} \dots \kappa_{\xi_{j_k}} \tilde{G}(\mu', \Sigma')[\kappa] = \\ \partial_{\tilde{J}_{j_1}} \dots \partial_{\tilde{J}_{j_n}} \int d\kappa \tilde{\mathcal{N}}(\nu, \Sigma)[- \kappa] e^{2\pi i \tilde{\mathbf{J}}^T \kappa} \tilde{\mathcal{N}}(\mu', \Sigma')[\kappa], \end{aligned} \quad (\text{A8})$$

where we have introduced a (dual) source term $e^{2\pi i \tilde{\mathbf{J}}^T \kappa}$, in the same flavor of what already done in direct space. The integral term in Eq. (A8) can then be rewritten as:

$$\begin{aligned} \int d\kappa \tilde{\mathcal{N}}(\nu, \Sigma)[- \kappa] e^{2\pi i \tilde{\mathbf{J}}^T \kappa} \tilde{\mathcal{N}}(\mu', \Sigma')[\kappa] = \\ \int d\kappa e^{2\pi i \kappa^T \nu} e^{-2\pi^2 \kappa^T \Sigma \kappa} e^{2\pi i \tilde{\mathbf{J}}^T \kappa} e^{-2\pi i \kappa^T \mu'} e^{-2\pi^2 \kappa^T \Sigma' \kappa} = \\ \int d\kappa e^{-2\pi i \kappa^T (\mu' - \nu - \tilde{\mathbf{J}})} e^{-2\pi^2 \kappa^T (\Sigma + \Sigma') \kappa}. \end{aligned} \quad (\text{A9})$$

Computing the integral, this last equation can be cast as:

$$\begin{aligned} \int d\kappa \tilde{\mathcal{N}}(\nu, \Sigma)[- \kappa] e^{2\pi i \tilde{\mathbf{J}}^T \kappa} \tilde{\mathcal{N}}(\mu', \Sigma')[\kappa] = \\ \frac{1}{\sqrt{(2\pi)^M \det(\Sigma + \Sigma')}} \exp\left[-\frac{1}{2} \zeta^T (\Sigma + \Sigma')^{-1} \zeta\right], \end{aligned} \quad (\text{A10})$$

where we defined the quantity $\zeta = \zeta(\mathbf{J}, \tilde{\mathbf{J}})$ as:

$$\zeta(\mathbf{J}, \tilde{\mathbf{J}}) := \mu' - \mu - \mathbf{J}^T \Sigma - \tilde{\mathbf{J}}. \quad (\text{A11})$$

Oftentimes, as mentioned in the main text, it is convenient to work with complex Gaussians. This assumption, in the Variational Multi-Gaussian (VMG) ansatz, makes us be able to capture negative features of the Wigner function such as interference phenomena. In the present work, this is achieved by considering an ansatz Wigner function given by the sum of the real parts of a set of complex Gaussians (cf. Eq. (5)), whose centers μ are allowed to also have an imaginary part: $\mu = \alpha + i\beta$. Effectively, the imaginary components of the centers act by re-modulating the Gaussian by a sinusoidal component, thus allowing negative values. The choice of taking the real parts of complex Gaussians is not arbitrary. Indeed, while the real part of a complex Gaussian retains the normalization condition of a proper quasiprobability density function, the norm of the imaginary part is instead zero. In this case the generalized Gaussian moments can be computed as derivatives of a generating function $\mathcal{Z}[\mathbf{J}, \tilde{\mathbf{J}}]$:

$$\begin{aligned} \langle \xi_{i_1} \dots \xi_{i_l} \partial_{\xi_{j_1}} \dots \partial_{\xi_{j_k}} \rangle_{(\mu, \Sigma), (\mu', \Sigma')} = \\ \partial_{J_{i_1}} \dots \partial_{J_{i_l}} \partial_{\tilde{J}_{j_1}} \dots \partial_{\tilde{J}_{j_k}} \mathcal{Z}[\mathbf{J}, \tilde{\mathbf{J}}]. \end{aligned} \quad (\text{A12})$$

Specifically, $\mathcal{Z}[\mathbf{J}, \tilde{\mathbf{J}}]$ has the form:

$$\mathcal{Z}[\mathbf{J}, \tilde{\mathbf{J}}] = \frac{\frac{1}{2} e^{\frac{1}{2} \mathbf{J}^T \Sigma \mathbf{J} + \mathbf{J}^T \boldsymbol{\alpha}}}{\sqrt{(2\pi)^M \det(\Sigma + \Sigma')}} \mathcal{Z}_1(\mathcal{M}_- \mathcal{C}_- + \mathcal{M}_+ \mathcal{C}_+), \quad (\text{A13})$$

where the function \mathcal{Z}_1 is defined as:

$$\mathcal{Z}_1 = \exp \left[-\frac{1}{2} (\boldsymbol{\alpha}' - \boldsymbol{\alpha} - \mathbf{J}^T \Sigma - \tilde{\mathbf{J}})^T (\Sigma + \Sigma')^{-1} (\boldsymbol{\alpha}' - \boldsymbol{\alpha} - \mathbf{J}^T \Sigma - \tilde{\mathbf{J}}) \right], \quad (\text{A14})$$

while the functions \mathcal{M}_- and \mathcal{M}_+ are:

$$\begin{aligned} \mathcal{M}_- &= \exp \left[\frac{1}{2} (\boldsymbol{\beta}' - \boldsymbol{\beta})^T (\Sigma + \Sigma')^{-1} (\boldsymbol{\beta}' - \boldsymbol{\beta}) \right], \\ \mathcal{M}_+ &= \exp \left[\frac{1}{2} (\boldsymbol{\beta}' + \boldsymbol{\beta})^T (\Sigma + \Sigma')^{-1} (\boldsymbol{\beta}' + \boldsymbol{\beta}) \right]. \end{aligned} \quad (\text{A15})$$

Finally, the functions \mathcal{C}_- and \mathcal{C}_+ are defined as:

$$\begin{aligned} \mathcal{C}_- &= \cos [\mathbf{J}^T \boldsymbol{\beta} - (\boldsymbol{\beta}' - \boldsymbol{\beta})^T (\Sigma + \Sigma')^{-1} (\boldsymbol{\alpha}' - \boldsymbol{\alpha} - \mathbf{J}^T \Sigma - \tilde{\mathbf{J}})], \\ \mathcal{C}_+ &= \cos [\mathbf{J}^T \boldsymbol{\beta} + (\boldsymbol{\beta}' + \boldsymbol{\beta})^T (\Sigma + \Sigma')^{-1} (\boldsymbol{\alpha}' - \boldsymbol{\alpha} - \mathbf{J}^T \Sigma - \tilde{\mathbf{J}})]. \end{aligned} \quad (\text{A16})$$

Appendix B: Phase space formulation of quantum mechanics

In the phase-space formulation of quantum mechanics, there exists a one-to-one correspondence between operators and functions on position-momentum coordinates. For any quantum operator $\hat{O}(\hat{q}, \hat{p})$ we can define its associated Weyl symbol $O_W(q, p)$ as [35]:

$$O_W(q, p) = \int d\xi \left\langle q - \frac{\xi}{2} \right| \hat{O}(\hat{q}, \hat{p}) \left| q + \frac{\xi}{2} \right\rangle e^{ip\xi/\hbar}. \quad (\text{B1})$$

The Wigner function, in turn, can be defined as the Weyl symbol of the density matrix $\hat{\rho}$:

$$W(q, p) = \int d\xi \hat{\rho}(q - \xi/2, q + \xi/2) e^{ip\xi/\hbar}. \quad (\text{B2})$$

More generally, Weyl symbols are functions of fundamental importance in the phase-space formulation of quantum mechanics. The expectation value of any operator is given by the average of the corresponding Weyl symbol over the Wigner function:

$$\langle \hat{O}(\hat{q}, \hat{p}) \rangle \equiv \text{Tr}[\hat{\rho} \hat{O}(\hat{q}, \hat{p})] = \int \frac{dq dp}{2\pi\hbar} W(q, p) O_W(q, p). \quad (\text{B3})$$

In order to introduce quantum dynamics in the phase-space formalism [72], we first need to introduce Moyal brackets $\{\circ, \circ\}_{MB}$ and the star product \star . We can define the star product between the Weyl symbol of an operator and the Wigner function as follows:

$$\begin{aligned} H_W \star W &= H_W \left(q + \frac{i\hbar}{2} \partial_p, p - \frac{i\hbar}{2} \partial_q \right) W, \\ W \star H_W &= H_W \left(q - \frac{i\hbar}{2} \partial_p, p + \frac{i\hbar}{2} \partial_q \right) W. \end{aligned} \quad (\text{B4})$$

Moyal bracket's $\{\circ, \circ\}_{MB}$ definition comes directly from the star product:

$$\{H, W\}_{MB} = -\frac{i}{\hbar} (H_W \star W - W \star H_W). \quad (\text{B5})$$

The Lindblad master equation in phase space can be reformulated as follows:

$$\frac{\partial W(q, p)}{\partial t} = \{H_W, W\}_{MB} + \sum_j \gamma_j \mathcal{D}_{W_j}[W], \quad (\text{B6})$$

where H_W is the Weyl symbol of the Hamiltonian and $\{\circ, \circ\}_{MB}$ represents the Moyal bracket. Moreover the action of the phase space super-operators \mathcal{D}_{W_j} in the phase space, whose Weyl symbol for the jump operator is Γ_{W_j} , reads:

$$\begin{aligned} \mathcal{D}_j W &= \sum_k \Gamma_{W_{jk}} \star W \star \Gamma_{W_{jk}}^\dagger \\ &\quad - \frac{1}{2} \left((\Gamma_{W_{jk}}^\dagger \Gamma_{W_{jk}}) \star W + W \star (\Gamma_{W_{jk}}^\dagger \Gamma_{W_{jk}}) \right). \end{aligned} \quad (\text{B7})$$

By a quick comparison with the Lindblad master equation for the density matrix (Eq. (1)), it is possible to notice how the Moyal brackets replace the commutator, the Weyl symbols take the place of the operators, and the Wigner function fill in for the density matrix $\hat{\rho}$.

1. Bose-Hubbard Lindbladian in phase-space

Let us now consider a M -modes (sites) driven dissipative Bose-Hubbard Hamiltonian (Eq. (17)) which we also report here for the sake of simplicity:

$$\begin{aligned} \hat{H} &= \sum_{j=1}^{N_G} \left[-\Delta \hat{a}_j^\dagger \hat{a}_j + \frac{U}{2} \hat{a}_j^{\dagger 2} \hat{a}_j^2 + \frac{G}{2} \hat{a}_j^{\dagger 2} + \frac{G^*}{2} \hat{a}_j^2 \right] \\ &\quad - \sum_{\langle j, j' \rangle} \frac{J}{z} (\hat{a}_j^\dagger \hat{a}_{j'} + \hat{a}_j \hat{a}_{j'}^\dagger). \end{aligned} \quad (\text{B8})$$

For clarity, we will denote by $\mathcal{L}_G W$ the explicit result of Eq. (B6) comprising only the terms proportional to the double-boson driving amplitude G . We use an analogous notation for all the other terms in the Hamiltonian. By explicitly computing Eq. (B6) one finds:

$$\mathcal{L}_G W = \sum_{j=1}^M \left[\text{Re}[G] \left(p_j \frac{\partial W}{\partial q_j} + q_j \frac{\partial W}{\partial p_j} \right) - \text{Im}[G] \left(q_j \frac{\partial W}{\partial q_j} - p_j \frac{\partial W}{\partial p_j} \right) \right], \quad (\text{B9})$$

$$\mathcal{L}_\Delta W = \Delta \sum_{j=1}^M \left[p_j \frac{\partial W}{\partial q_j} - q_j \frac{\partial W}{\partial p_j} \right], \quad (\text{B10})$$

$$\begin{aligned} \mathcal{L}_U W = \frac{U}{2} \sum_{j=1}^M & \left[(q_j^2 + p_j^2) \left(q_j \frac{\partial W}{\partial p_j} - p_j \frac{\partial W}{\partial q_j} \right) \right. \\ & + 2 \left(p_j \frac{\partial W}{\partial q_j} - q_j \frac{\partial W}{\partial p_j} \right) \\ & + \frac{1}{4} \left(p_j \frac{\partial^3 W}{\partial q_j^3} - q_j \frac{\partial^3 W}{\partial p_j^3} \right. \\ & \left. \left. - q_j \frac{\partial^3 W}{\partial p_j \partial q_j^2} + p_j \frac{\partial^3 W}{\partial q_j \partial p_j^2} \right) \right], \quad (\text{B11}) \end{aligned}$$

$$\begin{aligned} \mathcal{L}_J W = & -\frac{J}{z} \sum_{\langle j,j' \rangle} \left[q_j \frac{\partial}{\partial p_{j'}} + q_{j'} \frac{\partial}{\partial p_j} - p_j \frac{\partial}{\partial q_{j'}} - p_{j'} \frac{\partial}{\partial q_j} \right] W. \quad (\text{B12}) \end{aligned}$$

In a similar way one can also compute the terms corresponding to the single and two-boson dissipations:

$$\begin{aligned} \mathcal{L}_\gamma W = \frac{\gamma}{2} \sum_{j=1}^M & \left[q_j \frac{\partial W}{\partial q_j} + p_j \frac{\partial W}{\partial p_j} \right. \\ & \left. + 2W + \frac{1}{2} \frac{\partial^2 W}{\partial q_j^2} + \frac{1}{2} \frac{\partial^2 W}{\partial p_j^2} \right], \quad (\text{B13}) \end{aligned}$$

$$\begin{aligned} \mathcal{L}_\eta W = \frac{\eta}{2} \sum_{j=1}^M & \left[\left((q_j^3 + q_j p_j^2) \frac{\partial W}{\partial q_j} \right. \right. \\ & \left. + (p_j^3 + q_j^2 p_j) \frac{\partial W}{\partial p_j} \right) \\ & + 2\eta ((q_j^2 + p_j^2)W) + \eta \left(q_j \frac{\partial W}{\partial q_j} + p_j \frac{\partial W}{\partial p_j} \right) \\ & + \frac{\eta}{2} \left((q_j^2 + p_j^2) \left(\frac{\partial^2 W}{\partial q_j^2} + \frac{\partial^2 W}{\partial p_j^2} \right) \right) \\ & + \frac{\eta}{8} \left(q_j \frac{\partial^3 W}{\partial q_j^3} + p_j \frac{\partial^3 W}{\partial p_j^3} + q_j \frac{\partial}{\partial p_j} \left(\frac{\partial^2 W}{\partial p_j^2} \right) \right. \\ & \left. \left. + p_j \frac{\partial}{\partial p_j} \left(\frac{\partial^2 W}{\partial q_j^2} \right) \right) \right]. \quad (\text{B14}) \end{aligned}$$

2. Parity Weyl symbol

In this subsection, we calculate the Weyl symbol corresponding to the boson number parity operator $\hat{\Pi} = \exp(i\pi \sum_i \hat{a}_i^\dagger \hat{a}_i)$.

The parity operator $\hat{\Pi}$ acts on the position and momentum basis as [73]:

$$\hat{\Pi}|q\rangle = |-q\rangle; \quad \hat{\Pi}|p\rangle = |-p\rangle. \quad (\text{B15})$$

The Weyl symbol of the parity operator $\hat{\Pi}$ of a 1-mode bosonic system can be computed directly from the definition Eq. (B1):

$$\begin{aligned} \Pi_W(x,p) &= \int d\xi \left\langle x - \frac{\xi}{2} | \hat{\Pi} | x + \frac{\xi}{2} \right\rangle e^{ip\xi/\hbar} \\ &= \int d\xi \delta(2x) \frac{2\pi}{2\pi} e^{ip\xi/\hbar} \\ &= \frac{\delta(x)}{2} \delta(p) 2\pi = \pi \delta(x) \delta(p). \quad (\text{B16}) \end{aligned}$$

In the phase-space formalism, the expectation value of the parity operator on the whole system is thus simply given by π times the value of the Wigner function at the center of the phase space. Analogously, for a system of n -bosonic sites, we have found that it is given by:

$$\Pi_W(\mathbf{q}, \mathbf{p}) = \pi^n \delta(\mathbf{q}) \delta(\mathbf{p}). \quad (\text{B17})$$

Appendix C: Squeezed Coherent states

In a Gaussian function [Eq. (6)], the covariance matrix Σ is of profound importance, as it determines the extent to which the function is squeezed along one direction relative to another. We have seen in the previous paragraph that the parity expectation value is determined by the value of the Wigner function in the origin of the phase-space. If we now imagine to have a Gaussian centered in zero and to arbitrarily reduce its covariance matrix -which controls the broadness of the Gaussian- its peak in zero will become higher and higher. Once the peak of the Gaussian overcomes the value of $1/\pi$, the parity expectation value would exceed one, thus violating the Heisenberg uncertainty principle. In this paragraph we introduce all the key elements and the basic notions to parametrize a physical covariance matrix for Gaussian quantum states.

Let us consider an M -modes bosonic system with annihilation and creation operators obeying the standard commutation relations:

$$\begin{aligned} [\hat{a}_j, \hat{a}_k^\dagger] &= \delta_{jk}, \\ [\hat{a}_j, \hat{a}_k] &= [\hat{a}_j^\dagger, \hat{a}_k^\dagger] = 0. \quad (\text{C1}) \end{aligned}$$

It is usually convenient to introduce the Hermitian real quadrature operators:

$$\hat{q}_k = \frac{1}{\sqrt{2}} (\hat{a}_k + \hat{a}_k^\dagger), \quad \hat{p}_k = \frac{1}{i\sqrt{2}} (\hat{a}_k - \hat{a}_k^\dagger), \quad (\text{C2})$$

which satisfy:

$$\begin{aligned} [\hat{q}_j, \hat{p}_k] &= i\delta_{jk}, \\ [\hat{q}_j, \hat{q}_k] &= [\hat{p}_j, \hat{p}_k] = 0. \end{aligned} \quad (\text{C3})$$

If we arrange these real quadrature into the following vector [74]:

$$\hat{\xi} = \begin{pmatrix} \hat{q}_1 \\ \hat{p}_1 \\ \vdots \\ \hat{q}_M \\ \hat{p}_M \end{pmatrix}, \quad (\text{C4})$$

the canonical commutation relation can thus be rewritten as:

$$[\hat{\xi}_k, \hat{\xi}_l] = i\Omega_{kl}. \quad (\text{C5})$$

Here Ω is the symplectic matrix defined as

$$\Omega = \bigoplus_{k=1}^{2M} \begin{pmatrix} 0 & 1 \\ -1 & 0 \end{pmatrix} = \mathbb{1}_M \otimes \begin{pmatrix} 0 & 1 \\ -1 & 0 \end{pmatrix}. \quad (\text{C6})$$

The covariance matrix of a generic pure Gaussian state can be written as:

$$\Sigma_{kl} = \frac{1}{2} \langle \{\hat{\xi}_k, \hat{\xi}_l\} \rangle - \langle \hat{\xi}_k \rangle \langle \hat{\xi}_l \rangle. \quad (\text{C7})$$

In order to be physical, it is well known that the covariance matrix has to respect the following inequality [74]:

$$\Sigma + \frac{i}{2}\Omega \geq 0. \quad (\text{C8})$$

In general, checking the validity of Eq. (C8) for a generic covariance matrix Σ is a difficult task. In order to overcome this issue we construct a physical covariance matrix by applying squeezing and displacement operators [75]. Namely, a squeezed coherent state is defined as

$$|\alpha, \zeta\rangle = \hat{D}(\alpha)\hat{S}(\zeta)|0\rangle, \quad (\text{C9})$$

where $|0\rangle$ is the vacuum state, while \hat{D} and \hat{S} are respectively the displacement and the squeezing operator:

$$\begin{aligned} \hat{D}(\alpha) &= \prod_{j=1}^M \exp(\alpha_j \hat{a}_j^\dagger - \alpha_j^* \hat{a}_j), \\ \hat{S}(\zeta) &= \prod_{j=1}^M \exp\left[\frac{1}{2}(\zeta_j^* \hat{a}_j^2 - \zeta_j \hat{a}_j^{\dagger 2})\right]. \end{aligned} \quad (\text{C10})$$

Both these operations are symplectic, i.e. Ω is left invariant under their action: $\hat{S}^T \Omega \hat{S} = \Omega$ and $\hat{D}^T \Omega \hat{D} = \Omega$. This implies that any state whose covariance matrix Σ is obtained through displacement and squeezing operations respects the inequality Eq. (C8) [46, 74]. Specifically, the covariance matrix of the single-mode vacuum state

($\Sigma_{VAC} = \mathbb{1}_2/2$) is transformed by the squeezing operator $\hat{S}(\zeta = re^{i\phi})$ as [45]:

$$\Sigma(\zeta) = \frac{1}{2} \cosh(2r) \mathbb{1}_2 - \frac{1}{2} \sinh(2r) \mathbf{S}_\phi, \quad (\text{C11})$$

where

$$\mathbf{S}_\phi = \begin{pmatrix} \cos(\phi) & \sin(\phi) \\ \sin(\phi) & -\cos(\phi) \end{pmatrix}. \quad (\text{C12})$$

The displacement operator leaves the covariance matrix unchanged.

Appendix D: Variational Multi-Gaussian parametrization

In this section we expose how we parametrize the Variational Multi-Gaussian (VMG) ansatz for the Wigner function and we discuss how the number of variational parameters scales with the number of Gaussians (N_G) and the number of bosonic modes (M).

The vector θ includes all the ansatz variational parameters, namely the normalization coefficients c_i , the centers μ_i and the squeezing parameters ζ_i , where the index i ranges from 1 to N_G .

Since the Liouvillian terms considered in this work are invariant under the transformation $\hat{a}_j \rightarrow -\hat{a}_j$ and $\hat{a}_j^\dagger \rightarrow -\hat{a}_j^\dagger$, the quantum master equation preserves the phase-space parity of the Wigner function ($W(\mathbf{q}, \mathbf{p}) = W(-\mathbf{q}, -\mathbf{p})$). Since the steady state is also expected to be an even phase-space function, we consider a variational ansatz given by:

$$\begin{aligned} W(\xi; \theta) &\equiv \sum_{i=1}^{N_G} \text{Re} \left[G(\xi; \theta_i = (c_i, \mu_i, \Sigma_i)) \right. \\ &\quad \left. + G(\xi; \theta_i = (c_i, -\mu_i, \Sigma_i)) \right], \end{aligned} \quad (\text{D1})$$

which is explicitly even. Moreover, the centers of the Gaussians are assumed to be complex: $\mu = \alpha + i\beta$ in order to capture negative features. To parameterize the ansatz for $2N_G$ Gaussian functions, we need N_G real parameters for the normalization coefficients, and $N_G \times 4M$ real parameters for the real and the imaginary parts of the centers.

In the case of a many mode system we initialized the covariance matrices Σ_i as a block diagonal matrices in which every block is determined by M -couples of parameters encoding M -single-mode squeezing operations on the vacuum state: (\mathbf{r}, ϕ) , where $\mathbf{r} = (r_1, \dots, r_M)$ and $\phi = (\phi_1, \dots, \phi_M)$ [cf. Eq. (C12)]. While multi-mode correlations are still guaranteed by the presence of many Gaussian functions with different weights c_i , this parametrization scales linearly with the number of Gaussian functions. For the considered case of bi-Gaussians, in order to encode the covariance matrices of $2N_G$ Gaussians, we need $N_G \times 2M$ real parameters.

Eventually, to fully encode $2N_G$ Gaussians we thus need a total number of $6N_G \times (M+1/6)$ variational parameters. For example, to compute the dynamics of a 144 bosonic sites with 16 Gaussians, we unraveled the dynamical evolution of 6920 parameters. This approach scales linearly both in the number N_G of Gaussians and in the number M of bosonic modes considered.

-
- [1] I. Carusotto and C. Ciuti, Quantum fluids of light, *Rev. Mod. Phys.* **85**, 299 (2013).
- [2] T. Ozawa, H. M. Price, A. Amo, N. Goldman, M. Hafezi, L. Lu, M. C. Rechtsman, D. Schuster, J. Simon, O. Zilberberg, and I. Carusotto, Topological photonics, *Rev. Mod. Phys.* **91**, 015006 (2019).
- [3] I. Carusotto, A. A. Houck, A. J. Kollár, P. Roushan, D. I. Schuster, and J. Simon, Photonic materials in circuit quantum electrodynamics, *Nat. Phys.* **16**, 268 (2020).
- [4] M. Mirrahimi, Z. Leghtas, V. V. Albert, S. Touzard, R. J. Schoelkopf, L. Jiang, and M. H. Devoret, Dynamically protected cat-qubits: a new paradigm for universal quantum computation, *New J. Phys.* **16**, 045014 (2014).
- [5] Z. Leghtas, S. Touzard, I. M. Pop, A. Kou, B. Vlastakis, A. Petrenko, K. M. Sliwa, A. Narla, S. Shankar, M. J. Hatridge, M. Reagor, L. Frunzio, R. J. Schoelkopf, M. Mirrahimi, and M. H. Devoret, Confining the state of light to a quantum manifold by engineered two-photon loss, *Science* **347**, 853 (2015).
- [6] D. J. Weigand and B. M. Terhal, Generating grid states from Schrödinger-cat states without postselection, *Phys. Rev. A* **97**, 022341 (2018).
- [7] J. Guillaud and M. Mirrahimi, Repetition Cat Qubits for Fault-Tolerant Quantum Computation, *Phys. Rev. X* **9**, 041053 (2019).
- [8] A. Grimm, N. E. Frattini, S. Puri, S. O. Mundhada, S. Touzard, M. Mirrahimi, S. M. Girvin, S. Shankar, and M. H. Devoret, Stabilization and operation of a Kerr-cat qubit, *Nature* **584**, 205 (2020).
- [9] M. V. Larsen, X. Guo, C. R. Breum, J. S. Neergaard-Nielsen, and U. L. Andersen, Deterministic multi-mode gates on a scalable photonic quantum computing platform, *Nat. Phys.* **17**, 1018 (2021).
- [10] A. Joshi, K. Noh, and Y. Y. Gao, Quantum information processing with bosonic qubits in circuit QED, *Quantum Science and Technology* **6**, 033001 (2021).
- [11] R. Gautier, A. Sarlette, and M. Mirrahimi, Combined Dissipative and Hamiltonian Confinement of Cat Qubits, *PRX Quantum* **3**, 020339 (2022).
- [12] C. Chamberland, K. Noh, P. Arrangoiz-Arriola, E. T. Campbell, C. T. Hann, J. Iverson, H. Putterman, T. C. Bohdanowicz, S. T. Flammia, A. Keller, G. Refael, J. Preskill, L. Jiang, A. H. Safavi-Naeini, O. Painter, and F. G. Brandão, Building a Fault-Tolerant Quantum Computer Using Concatenated Cat Codes, *PRX Quantum* **3**, 010329 (2022).
- [13] X. Pan, J. Schwinger, N.-N. Huang, P. Song, W. Chua, F. Hanamura, A. Joshi, F. Valadares, R. Filip, and Y. Y. Gao, Protecting the Quantum Interference of Cat States by Phase-Space Compression, *Phys. Rev. X* **13**, 021004 (2023).
- [14] A. Hajr, B. Qing, K. Wang, G. Koolstra, Z. Pedramrazi, Z. Kang, L. Chen, L. B. Nguyen, C. Jünger, N. Goss, I. Huang, B. Bhandari, N. E. Frattini, S. Puri, J. Dressel, A. N. Jordan, D. I. Santiago, and I. Siddiqi, High-Coherence Kerr-Cat Qubit in 2D Architecture, *Phys. Rev. X* **14**, 041049 (2024).
- [15] A. Marquet, A. Essig, J. Cohen, N. Cottet, A. Murani, E. Albertinale, S. Dupouy, A. Bienfait, T. Peronnin, S. Jezouin, R. Lescanne, and B. Huard, Autoparametric Resonance Extending the Bit-Flip Time of a Cat Qubit up to 0.3 s, *Phys. Rev. X* **14**, 021019 (2024).
- [16] A. Z. Ding, B. L. Brock, A. Eickbusch, A. Koottandavida, N. E. Frattini, R. G. Cortiñas, V. R. Joshi, S. J. de Graaf, B. J. Chapman, S. Ganjam, L. Frunzio, R. J. Schoelkopf, and M. H. Devoret, Quantum control of an oscillator with a Kerr-cat qubit, *Nat. Commun.* **16**, 5279 (2025).
- [17] H. Hutin, P. Bilous, C. Ye, S. Abdollahi, L. Cros, T. Dvir, T. Shah, Y. Cohen, A. Bienfait, F. Marquardt, and B. Huard, Preparing Schrödinger Cat States in a Microwave Cavity Using a Neural Network, *PRX Quantum* **6**, 010321 (2025).
- [18] M. Yuan, A. Seif, A. Lingenfelter, D. I. Schuster, A. A. Clerk, and L. Jiang, Universal control in bosonic systems with weak Kerr nonlinearities, *Phys. Rev. A* **111**, 032606 (2025).
- [19] U. Schollwöck, The density-matrix renormalization group in the age of matrix product states, *Ann. Phys.* **326**, 96 (2011).
- [20] R. Orús, Tensor networks for complex quantum systems, *Nat. Rev. Phys.* **1**, 538 (2019).
- [21] D. Kilda, A. Biella, M. Schirò, R. Fazio, and J. Keeling, On the stability of the infinite Projected Entangled Pair Operator ansatz for driven-dissipative 2D lattices, *SciPost Phys. Core* **4**, 005 (2021).
- [22] D. A. Hryniuk and M. H. Szymańska, Tensor-network-based variational Monte Carlo approach to the non-equilibrium steady state of open quantum systems, *Quantum* **8**, 1475 (2024).
- [23] S. Finazzi, A. Le Boité, F. Storme, A. Baksic, and C. Ciuti, Corner-space renormalization method for driven-dissipative two-dimensional correlated systems, *Phys. Rev. Lett.* **115**, 080604 (2015).
- [24] R. Rota, F. Minganti, C. Ciuti, and V. Savona, Quantum critical regime in a quadratically driven nonlinear photonic lattice, *Phys. Rev. Lett.* **122**, 110405 (2019).
- [25] G. Carleo and M. Troyer, Solving the quantum many-body problem with artificial neural networks, *Science* **355**, 602 (2017).
- [26] J. Carrasquilla and G. Torlai, How To Use Neural Networks To Investigate Quantum Many-Body Physics, *PRX Quantum* **2**, 040201 (2021).
- [27] F. Vicentini, A. Biella, N. Regnault, and C. Ciuti, Variational Neural-Network Ansatz for Steady States in Open Quantum Systems, *Phys. Rev. Lett.* **122**, 250503 (2019).
- [28] M. J. Hartmann and G. Carleo, Neural-Network Approach to Dissipative Quantum Many-Body Dynamics, *Phys. Rev. Lett.* **122**, 250502 (2019).
- [29] N. Yoshioka and R. Hamazaki, Constructing neural stationary states for open quantum many-body systems, *Phys. Rev. B* **99**, 214306 (2019).
- [30] A. Nagy and V. Savona, Variational Quantum Monte Carlo Method with a Neural-Network Ansatz for Open Quantum Systems, *Phys. Rev. Lett.* **122**, 250501 (2019).
- [31] G. Torlai, G. Mazzola, J. Carrasquilla, M. Troyer, R. Melko, and G. Carleo, Neural-network quantum state tomography, *Nat. Phys.* **14**, 447 (2018).
- [32] F. Carnazza, F. Carollo, D. Zietlow, S. Andergassen, G. Martius, and I. Lesanovsky, Inferring Markovian quantum master equations of few-body observables in interacting spin chains, *New J. Phys.* **24**, 073033 (2022).

- [33] D. Luo, Z. Chen, J. Carrasquilla, and B. K. Clark, Autoregressive Neural Network for Simulating Open Quantum Systems via a Probabilistic Formulation, *Phys. Rev. Lett.* **128**, 090501 (2022).
- [34] Z. Denis and G. Carleo, Accurate neural quantum states for interacting lattice bosons, *Quantum* **9**, 1772 (2025).
- [35] A. Polkovnikov, Phase space representation of quantum dynamics, *Ann. Phys. (N. Y.)* **325**, 1790 (2010).
- [36] P. Deuar, A. Ferrier, M. Matuszewski, G. Orso, and M. H. Szymańska, Fully Quantum Scalable Description of Driven-Dissipative Lattice Models, *PRX Quantum* **2**, 010319 (2021).
- [37] C. C. Margossian, A review of automatic differentiation and its efficient implementation, *WIREs Data Min. Knowl. Discov.* **9**, e1305 (2019).
- [38] A. Griewank and A. Walther, *Evaluating Derivatives: Principles and Techniques of Algorithmic Differentiation*, 2nd ed. (SIAM, 2008).
- [39] H. Breuer and F. Petruccione, *The Theory of Open Quantum Systems*, 1st ed. (Oxford University Press, Great Clarendon Street, Oxford, UK, 2002) p. 648.
- [40] E. Wigner, On the Quantum Correction For Thermodynamic Equilibrium, *Phys. Rev.* **40**, 749 (1932).
- [41] R. J. Glauber, Coherent and incoherent states of the radiation field, *Phys. Rev.* **131**, 2766 (1963).
- [42] E. C. G. Sudarshan, Equivalence of semiclassical and quantum mechanical descriptions of statistical light beams, *Phys. Rev. Lett.* **10**, 277 (1963).
- [43] K. Husimi, Some Formal Properties of the Density Matrix, *Proc. Phys.-Math. Soc. Jpn., 3rd Ser.* **22**, 264 (1940).
- [44] A. G. Baydin, B. A. Pearlmutter, A. A. Radul, and J. M. Siskind, Automatic differentiation in machine learning: a survey, *J. Mach. Learn. Res.* **18**, 1 (2018).
- [45] J. E. Bourassa, N. Quesada, I. Tzitrin, A. Száva, T. Isaacsson, J. Izaac, K. K. Sabapathy, G. Dauphinais, and I. Dhand, Fast Simulation of Bosonic Qubits via Gaussian Functions in Phase Space, *PRX Quantum* **2**, 040315 (2021).
- [46] M. Walschaers, Non-Gaussian Quantum States and Where to Find Them, *PRX Quantum* **2**, 030204 (2021).
- [47] Z. Leghtas, G. Kirchmair, B. Vlastakis, R. J. Schoelkopf, M. H. Devoret, and M. Mirrahimi, Hardware-efficient autonomous quantum memory protection, *Phys. Rev. Lett.* **111**, 120501 (2013).
- [48] B. Yurke and D. Stoler, Generating quantum mechanical superpositions of macroscopically distinguishable states via amplitude dispersion, *Phys. Rev. Lett.* **57**, 13 (1986).
- [49] O. Castaños, R. Jáuregui, R. López-Peña, J. Recamier, and V. I. Man'ko, Schrödinger-cat states in Paul traps, *Phys. Rev. A* **55**, 1208 (1997).
- [50] K. Vogel and H. Risken, Determination of quasiprobability distributions in terms of probability distributions for the rotated quadrature phase, *Phys. Rev. A* **40**, 2847 (1989).
- [51] Y.-F. Qu, M. Stefanini, T. Shi, T. Esslinger, S. Gopalakrishnan, J. Marino, and E. Demler, Variational approach to the dynamics of dissipative quantum impurity models, *Phys. Rev. B* **111**, 155113 (2025).
- [52] J. Bettencourt, M. J. Johnson, and D. K. Duvenaud, Taylor-Mode Automatic Differentiation for Higher-Order Derivatives in JAX (2019).
- [53] J. Bradbury, R. Frostig, P. Hawkins, M. J. Johnson, C. Leary, D. Maclaurin, G. Necula, A. Paszke, J. VanderPlas, S. Wanderman-Milne, and Q. Zhang, *JAX: composable transformations of Python+NumPy programs* (2018).
- [54] X. Yuan, S. Endo, Q. Zhao, Y. Li, and S. C. Benjamin, Theory of variational quantum simulation, *Quantum* **3**, 191 (2019).
- [55] D. Eeltink, F. Vicentini, and V. Savona, *Variational dynamics of open quantum systems in phase space* (2023), [arXiv:2307.07429 \[quant-ph\]](https://arxiv.org/abs/2307.07429).
- [56] A. Griewank, J. Utke, and A. Walther, Evaluating higher derivative tensors by forward propagation of univariate Taylor series, *Math. Comput.* **69**, 1117 (2000).
- [57] F. Dangel, T. Siebert, M. Zeinhofer, and A. Walther, Collapsing Taylor Mode Automatic Differentiation (2025), [arXiv:2505.13644 \[cs.LG\]](https://arxiv.org/abs/2505.13644).
- [58] L. Gravina, F. Minganti, and V. Savona, Critical Schrödinger Cat Qubit, *PRX Quantum* **4**, 020337 (2023).
- [59] J. Johansson, P. Nation, and F. Nori, QuTiP: An open-source Python framework for the dynamics of open quantum systems, *Comput. Phys. Commun.* **183**, 1760 (2012).
- [60] N. Bartolo, F. Minganti, W. Casteels, and C. Ciuti, Exact steady state of a Kerr resonator with one- and two-photon driving and dissipation: Controllable Wigner-function multimodality and dissipative phase transitions, *Phys. Rev. A* **94**, 033841 (2016).
- [61] C.-H. Chang, V. Dommes, R. Erramilli, A. Homrich, P. Kravchuk, A. Liu, M. Mitchell, D. Poland, and D. Simmons-Duffin, Bootstrapping the 3d Ising stress tensor, *J. High Energy Phys.* **2025** (3), 136.
- [62] M. Reehorst, *J. High Energy Phys.* **2022** (9), 177.
- [63] Z. Komargodski and D. Simmons-Duffin, The Random-Bond Ising Model in 2.01 and 3 Dimensions, *J. Phys. A: Math. Theor.* **50**, 154001 (2017).
- [64] A. Aspuru-Guzik and P. Walther, Photonic quantum simulators, *Nat. Phys.* **8**, 285 (2012).
- [65] J. Tosca, M. C. Strinati, C. Conti, and C. Ciuti, Emergent Equilibrium in All-Optical Single Quantum-Trajectory Ising Machines, *Phys. Rev. Lett.* **134**, 230404 (2025).
- [66] M. P. Fisher, P. B. Weichman, G. Grinstein, and D. S. Fisher, Boson localization and the superfluid-insulator transition, *Phys. Rev. B* **40**, 546 (1989).
- [67] J. Cardy, *Scaling and Renormalization in Statistical Physics*, Cambridge Lecture Notes in Physics (Cambridge University Press, 1996).
- [68] F. Minganti, A. Biella, N. Bartolo, and C. Ciuti, Spectral theory of Liouvillians for dissipative phase transitions, *Phys. Rev. A* **98**, 042118 (2018).
- [69] F. Vicentini, F. Minganti, R. Rota, G. Orso, and C. Ciuti, Critical slowing down in driven-dissipative Bose-Hubbard lattices, *Phys. Rev. A* **97**, 013853 (2018).
- [70] W. Verstraelen, R. Rota, V. Savona, and M. Wouters, Gaussian trajectory approach to dissipative phase transitions: The case of quadratically driven photonic lattices, *Phys. Rev. Res.* **2**, 022037 (2020).
- [71] L. Adzhemyan, D. Evdokimov, M. Hnatič, E. Ivanova, M. Kompaniets, A. Kudlis, and D. Zakharov, The dynamic critical exponent z for 2d and 3d Ising models from five-loop ϵ expansion, *Phys. Lett. A* **425**, 127870 (2022).
- [72] K. Vogel and H. Risken, Quasiprobability distributions in dispersive optical bistability, *Phys. Rev. A* **39**, 4675 (1989).
- [73] S. Haroche and J. M. Raimond, *Exploring the Quantum: Atoms, Cavities, and Photons* (Oxford Univ. Press, Ox-

- ford, 2006).
- [74] R. Simon, N. Mukunda, and B. Dutta, Quantum-noise matrix for multimode systems: $U(n)$ invariance, squeezing, and normal forms, [Phys. Rev. A](#) **49**, 1567 (1994).
- [75] D. F. Walls and G. J. Milburn, *Quantum Optics*, 2nd ed. (Springer, 2008).